
# UNIVERSIDAD NACIONAL AUTÓNOMA DE MÉXICO

POSGRADO EN CIENCIA E INGENIERÍA DE MATERIALES

INSTITUTO DE INVESTIGACIONES EN MATERIALES

## POLY (VINYL ALCOHOL) ELECTROSPUN NANOFIBERS LOADED WITH POLY (D,L-LACTIDE-CO-GLYCOLIDE) NANOPARTICLES AS A PROMISING TO EMBEDDED IN POLY LACTIC BIMODAL SCAFFOLDS WITH POTENTIAL IN TISSUE ENGINEERING

**T E S I S**

QUE PARA OPTAR POR EL GRADO DE:

MAESTRA EN CIENCIA E INGENIERÍA DE MATERIALES

**PRESENTA**

**ING. LINDA KATHERYN ORTIZ GIRON**

**TUTOR PRINCIPAL:**
DR. RICARDO VERA GRAZIANO
INSTITUTO DE INVESTIGACIONES EN MATERIALES, UNAM

**COMITÉ TUTOR:**
DR. MIKHAIL ZOLOTUKHIN
INSTITUTO DE INVESTIGACIONES EN MATERIALES, UNAM

DR. JOSE JUAN ESCOBAR CHAVEZ
FACULTAD DE ESTUDIOS SUPERIORES CUAUTITLAN, UNAM

CIUDAD UNIVERSITARIA, CIUDAD DE MÉXICO, SEPTIEMBRE, 2022

"Normality is a paved road. It is easy to walk but no flowers grow on it."
*Vincent Van Gogh.*

# Dedication

To my parents, Piedad and José Ignacio. To my sister Vanessa, my brothers Juan Camilo and Sebastián, my niece Luciana, my aunt Elsy and my best friend Edwin. To you, who have given me the motivation, strength, and support, I dedicate the culmination of this work with deep love.

# Acknowledgements

To Consejo Nacional de Ciencia y Tecnología (CONACyT) for funding and support for this work, as well as my living expenses during my stay in Mexico. To postgraduate degree in materials science and engineering (PCeIM) from UNAM for supporting me with all the requirements and enrollment.

To CONACyT and UNAM for supporting this work with the Projects CF-19 No.140617 and PAPIIT-IG100220, respectively.

To my advisor, Dr. Ricardo Vera Graziano for supporting me at all times with the necessary tools and requirements to develop this thesis.

I would like to express my sincere gratitude to Dr. Ciro Rodríguez for allowing me to do my research internship at the Tecnológico de Monterrey in the advanced manufacturing research group. As well as his work team, Dr. Víctor Segura-Ibarra and Dr. Raquel Tejeda Alejandre who accompanied me in this process. Thank you for the funding, infrastructure, and support necessary to develop this thesis.

I would like to highlight the work of Dr. Víctor Segura-Ibarra and Dr. Raquel Tejeda Alejandre. I will be infinitely grateful for their sincere advice, motivation, and exceptional accompaniment to make this work possible. I feel deeply grateful for all the knowledge, feedback and support they imparted to me to make possible this work.

To LCQ. Regina Vargas and Dr. Aída Rodríguez, for their constant support, motivation, and advice in the development of experiments and characterization of samples.

To my colleagues Erick and Angela Sánchez from the research group of Lab C202 of the IIM-UNAM for the support they gave me when I arrived in Mexico and for giving feedback on my work.

To my friends and colleagues Edwin, Gaby, Moy, and Mishai for all the personal growth they gave me in this process.

To Edwin Sebastian Barrera Mendivelso, who was not only my colleague but also my best friend and my family. To him, I want to express deep gratitude for his infinite patience, his advice, and his unconditional support and affection. His great advice filled me with perseverance.

To Thomas for his great support and motivation to complete this work during my stay

in Monterrey.

To my great friend, Juan Carlos Macias, who from a distance has always accompanied me with his advice and words of motivation for me to make the culmination of this work possible.

I want to thank my family for their unconditional support and for following this path by my side.

# Contents

# Abstract

Tissue engineering requires scaffold designs with tailored physical properties to achieve optimal performance. Additive manufacturing techniques have been widely used in tissue engineering and regenerative medicine, breaching the gap between biological and mechanical characteristics. These technologies enable the fabrication of scaffolds that mimic the macro and micro-environment of the native tissue. It has been proven that bimodal scaffolds can be manufactured with Fused Deposition Modeling and Electrospinning techniques. However, the development of multifunctional and hierarchically structured materials is still in demand for achieving successful tissue regeneration and facilitating drug delivery to ensure a rapid and efficient regeneration process *in situ*. Xanthohumol, one of the most interesting metabolites obtained from the hops (*Humulus lupulus* L.) has received growing attention due to its broad spectrum of biological activities and beneficial effects on human health. In this work, bimodal scaffolds were generated through the combination of FDM and ES, which has been focused on the validation of poly (vinyl alcohol) (PVA) electrospun nanofibers loaded with xanthohumol/poly (lactic-*co*-glycolic acid) nanoparticles (PLGA/XN).

The results showed the successful fabrication of the PVA electrospun nanofibers with PLGA/XN nanoparticles incorporated inside the fibers. In addition, the morphology characterization of the bimodal scaffolds showed that the meshes were successfully embedded into tridimensional poly lactic (PLA) constructs. The Cytotoxicity assay showed that the PVA electrospun nanofibers loaded with PLGA/XN nanoparticles are biocompatible. However, further studies to verify the potential osteoinduction of the bimodal scaffolds are needed.

# Publications

**Conference Presentations:**

- **Katheryn Ortiz-Giron**, Javier Vazquez-Armendariz, Victor Segura-Ibarra, Raquel Tejeda-Alejandre, Aida Rodriguez-Garcia, Ricardo Vera-Graziano, Ciro A. Rodriguez presented the contribution: *Fabrication of Poly Lactic Bimodal Scaffolds with Embedded PLGA-PVA Meshes For Tissue Engineering* as **oral modality**, in the F5. Materials for Health Applications: Biomaterials for Permanent and Temporary Implants, Dental, and Cosmetics Symposium at the XXX International Materials Research Congress and International Conference on Advanced Materials held in Cancun, Mexico from August 14th to 19th, 2022.

- **Katheryn Ortiz-Giron**, Ricardo Vera-Graziano presented the contribution: *Bimodal Scaffolds with Embedded PLGA-PVA Meshes For Tissue Engineering* as **oral modality** in the XXXV Congreso Nacional de la Sociedad Polimérica de México, AC in Monterrey, Nuevo León, México from october 17th to 21th, 2022.

- **Katheryn Ortiz-Giron**, Ricardo Vera-Graziano presented the contribution: *PVA/PLGA Nanofibers on PLA Meshes as Drug Carrier of Xanthohumol* as **poster modality**, in the XXXV Congreso Nacional de la Sociedad Polimérica de México, AC in Monterrey, Nuevo León, México from october 17th to 21th, 2022.

# List of Figures

# List of Tables

# List of Abreviations

| | |
|---|---|
| TE | Tissue Engineering |
| RM | Regenerative Medicine |
| ECM | Extracellular Matrix |
| 3D | Three-dimensional |
| ES | Electrospinning |
| AM | Additive Manufacturing |
| FDM | Fused Deposition Modeling |
| NPs | Nanoparticles |
| PCL | Polycaprolactone |
| PLA | Polylactic acid |
| PLGA | Poly (D,L-lactide-*co*-glycolide) |
| PVA | Polyvinyl Alcohol |
| XN | Xanthohumol |
| Rh | Rhodamine |
| DLS | Dynamic Light Scattering |
| SEM | Scanning Electron Microscopy |
| BSE | Backscattered Electrons |
| TEM | Transmission Electron Microscopy |
| FTIR | Fourier Transform Infrared Spectroscopy |
| ATR | Attenuated Total Reflectance |
| TGA | Thermogravimetric Analysis |

# Chapter 1

# Introduction

Regenerating damaged tissues or organs and restoring their functions has become a very active line of research, motivated mainly by its potential medical applications (Chun, Park, Kwon, & Khang, 2018). Recent advances in tissue engineering (TE) and regenerative medicine (RM) make it increasingly possible by integrating materials science, biomechanics, cell biology, and medical sciences (Auriemma et al., 2022). For instance, TE employs cells, scaffolds, and growth factors to regenerate or replace damaged or diseased tissue, while RM combines TE with other strategies, such as cell-based therapy, gene therapy, and immunomodulation to induce tissue/organ regeneration *in vivo* (Han et al., 2020).

The scaffolds are the key elements in TE. Since the cells needs a nest to promote the cell migration and to form the extracellular matrix (ECM), and to have an appropiate architecture to form the new tissue, while the scaffold is biodegraded. The geometric-property relationship derived from the manufacturing process allows scaffolds to perform successfully in tissue and organ regeneration (J. dos Santos et al., 2021; Dalton et al., 2013; Huang et al., 2020). There are several factors to consider when a scaffold is designed, such as i) porosity, ii) pore size, iii) pore interconnectivity, iv) mechanical properties, v) biocompatibility, vi) and biodegradation of the materials. Also, the physical-chemistry of the material surface (Wang et al., 2021; Hassan, Dave, Chandrawati, Dehghani, & Gomes, 2019).

Considering the complexity of the human body, TE must be focused on the designing and manufacturing of scaffolds with tailored properties and an architecture that mimics the macro- and microenvironment of the native tissue (Wang et al., 2021; Adel, ElMeligy, & Elkasabgy, 2022; Lara-Padilla, Mendoza-Buenrostro, Cardenas, Rodriguez-Garcia, & Rodriguez, 2017). This need has led to the combination of manufacturing techniques and the use of polymeric biomaterials as a promising approach. This is because a single fabrication technique will not be suitable for biomedical applications like therapeutic devices, including temporary prostheses, three-dimensional (3D) porous scaffolds, and delivery systems for pharmacological applications (Pouroutzidou et al., 2022; Adel et al., 2022).

An overview of the background and theory related to electrospinning, additive manufacturing, and the combination of both techniques for fabricating bimodal scaffolds and their applications is provided in this chapter. The motivation, problem, and objectives for

this experimental work are also described. Chapter 2 provides more detail on all materials and methods employed, while chapters 3 and 4 discuss the results and future works.

## 1.1 Motivation

Innovative solutions to improve the healthcare of the aging and diseased population remain a global challenge. To achieve this goal, TE and RM are emerging as promising approaches to meet the future needs of the patients. The purpose of TE is to develop a biodegradable matrix, commonly known as a scaffold, that can support tissue growth in three dimensions (3D) (Han et al., 2020). Multi-scale scaffolds with different architectures have been developed by using different polymeric materials and processing methodologies (Vazquez-Armendariz et al., 2020; Vyas et al., 2020; Lara-Padilla et al., 2017; Banche-Niclot et al., 2022). Recently, electrospinning and additive manufacturing as pioneering technologies to enable the preparation of multi-scale and multifunctional scaffolds with enhanced *in vitro* biological and tenable properties (Mohammadian & Eatemadi, 2017; Hassan et al., 2019). However, a fully characterized multifunctional scaffold system with tuneable physicochemical, morphological, mechanical, and biological properties is needed for tissue regeneration and drug delivery.

The motivation for this work was part of the research internship carried out at the *Tecnológico de Monterrey* as a result of the collaboration between the Tissue Engineering Research Group of the Dr. Ricardo Vera Graziano of the *Instituto de Investigaciones en Materiales-UNAM* and the Advanced Manufacturing Research Group of the Dr. Ciro A. Rodriguez of the *Tecnológico de Monterrey*. In previous works, the manufacturing of bimodal scaffolds fabricated by combining Electrospinning and Fused Deposition Modeling have been demostrated (Lara-Padilla et al., 2017; Vazquez-Armendariz et al., 2020). Due to all that, the elaboration and characterization of embedding electrospun nanofibers with nanoparticles that can release natural o synthetic drugs, in a controlled manner, inside the polymeric constructs performed by additive manufacturing could be interesting to explore. This is a promising approach to contributing to the regenerative capacity of the proposed bimodal scaffolds.

## 1.2 Background and Theory

### 1.2.1 Electrospinning, Additive Manufacturing, and Nanotechnology: A promising convergence

The fabrication of bimodal scaffolds has generated significant research interest in recent years, since one of the most difficult aspects of tissue engineering (TE) is the mimicry of the complex architecture of human tissue (L. Zhang, Yang, Johnson, & Jia, 2019; Dalton et al., 2013; Yu et al., 2016; Pina et al., 2019). Adapting scaffolds to real 3D environments for successful tissue regeneration remains a challenge (Kumar, Kumar, Tyagi, & Singh, 2022; Wang et al., 2021; Rajzer et al., 2018). The purpose of TE is to develop porous scaffolds, mechanically stable, and biocompatible that mimic the ECM as closely as possible to induce cell growth and differentiation both *in vitro* and *in vivo* (Han et al., 2020; J. dos Santos et al., 2021). As the nanofibers have a high surface-to-volume ratio that stimulates cell proliferation, the electrospinning (ES) technique has gained popularity in TE, since it mimic the structure and properties of the ECM (Saniei & Mousavi, 2020; Kumar et al., 2022; Jammalamadaka & Tappa, 2018).

Conventional and advanced techniques have been developed to fabricate 3D scaffolds, each one with its merits and drawbacks. For example, with conventional techniques such as Solvent Casting/Particulate Leaching (SC/PL), Melt Molding, Gas Foaming, Phase Separation, Freeze drying and Sol-gel transition, it is not possible to precisely control the size, geometry, and spatial distribution of the pores in the scaffolds (Adel et al., 2022). Advanced or Additive manufacturing (AM) techniques such as Stereolithography (SLA), Selective Laser Sintering (SLS), Fused Deposition Modeling (FDM), and Bioprinting have been developed (Saniei & Mousavi, 2020). These techniques use layer-by-layer deposition of materials to create tridimensional structures, offering advantages such as the control over the scaffold dimensions, porosity, interconnectivity, morphology, and chemical composition. However, the formation of large pores within the scaffold remains an important issue to overcome because it limits cell attachment and proliferation (Dalton et al., 2013; Ozbolat, 2015; Vyas et al., 2020; Smith & Mele, 2021). In this line, researchers have focused their efforts on manufacturing hybrid scaffolds with complex architecture that mimic the architecture of the ECM to overcome the shortcomings of each process (Puppi & Chiellini, 2020). For instance, ES and AM techniques have been combined to create hybrid scaffolds with nano and microscale structures to enhance cell activation. These structures, named bimodal scaffolds, have achieved promising results.

FDM is one of the most used 3D printing technologies to manufacture bimodal scaffolds since it is versatile, inexpensive, easy to operate, and does not require the use of solvents (Adel et al., 2022; Dalton et al., 2013; Mendoza-Buenrostro, Lara, & Rodriguez, 2015; Vazquez-Armendariz et al., 2020). The FDM process uses melted filament material to build complex geometries over a built platform, layer by layer, until a 3D object can be obtained. Firstly, the filament is supplied to the extrusion nozzle using drive wheels; secondly, the polymer melts in the extrusion nozzle until it is deposited on a construction platform, and finally, the extruder head is computer-controlled. This allows to construct the 3D layer by layer object (Moreno Madrid, Vrech, Sanchez, & Rodriguez, 2019). The layer thickness varies depending on the nozzle diameter. This method requires heating to melt the material, therefore its application is limited to the use of thermoplastic polymers,

such as polycaprolactone (PCL), polylactic acid (PLA), and poly(D,L-lactide-*co*-glycolide) (PLGA), which are biodegradable, non-toxic, biocompatible, and have excellent processing characteristics in terms of their mechanical strength and molecular weight (Adel et al., 2022; L. Zhang et al., 2019). Furthermore, these polymers have a relatively low melting point, are inexpensive, do not require post-processing to crosslink, and are widely available (Smith & Mele, 2021).

The combination of FDM with ES generates structures with macropores arranged in the form of a lattice that contains meshes formed by electrospun fibers between the different layers. Previous investigations have demonstrated the feasibility of fabricating these structures, named bimodal scaffolds (Dalton et al., 2013; Hassan et al., 2019; Smith & Mele, 2021; Rogers et al., 2014; Vazquez-Armendariz et al., 2020; Mendoza-Buenrostro et al., 2015; Naghieh, Foroozmehr, Badrossamay, & Kharaziha, 2017; Yu et al., 2016; Lara-Padilla et al., 2017; Centola et al., 2010; Adel et al., 2022; Rajzer et al., 2018). It is suggested that the electrospun nanofibers within the scaffolds provide morphological and biomechanical cues that can regulate the cell behavior and promote tissue regeneration.

In the work of Mota et al. (2011), electrospun nanofibers of PLGA were deposited on top of the PCL structures. The cytotoxicity test showed high viability and cell attachment into the hybrid scaffolds due to the presence of the meshes. According to Huang et al. (2020) and Vyas et al. (2020), a rotating drum electrospinning system combined with a screw-assisted extrusion 3D printer can be used to produce PCL structures with highly aligned nanofibers incorporated layer by layer as a promising approach for bone tissue regeneration. *In vitro* results showed that high-density electrospun meshes promoted the attachment of human adipose tissue-derived stem cells (hADSC) and enhanced their osteogenic differentiation. In the work of Lara-Padilla et al. (2017), the researchers manufactured PLA microfilaments with PCL electrospun fibers. The cytotoxicity assay perfomed on human fibroblasts showed a cell viability higher than 88%. By integrating PCL/gelatin nanofibers into the printing scaffold of PCL, a bimodal scaffold was created (Yu et al., 2016). The results showed that the cells exhibit a better migration and proliferation into the composite scaffolds, than those of PCL fabricated only by 3D printing. This could be due to the microporous structure of the electrospun scaffold. An overview of bimodal scaffolds developed by combining ES and AM techniques is given in **Table 1.1**. It has been demonstrated that bimodal scaffolds are breaching the gap between mechanical and biological properties. There is still a need for manufacturing bimodal scaffolds that better tailor specific applications and expand their scope areas. For example, for the controlled release of drugs and/or growth factors to help in tissue regeneration *in situ*.

It is important to note that the ES technique offers a significant advantage in fabricating bimodal scaffolds due to its ability to produce electrospun nanofiber meshes with an architecture that mimics the ECM of native tissues (Belgheisi, Haghbin Nazarpak, & Solati-Hashjin, 2022). Other remarkable features of these meshes include their high surface area, high porosity, flexibility, and an adjustable pore size distribution, including the fiber diameter and topography (Senthamizhan, Balusamy, & Uyar, 2017; Kumar et al., 2022; Wang et al., 2021). In addition, to manufacture the electrospun nanofibers a variety of biocompatible and/or biodegradable polymers can be used, including synthetic and natural polymers, and nanocomposites (Kumar et al., 2022). In contrast, scaffolds manufactured by AM techniques often use synthetic polymers which generally have a poor

biological activity and cellular affinity (Adel et al., 2022).

Advances in nanotechnology rekindled interest in electrospinning-related technologies in the mid-1990´s. ES is a versatile process to produce nano- and microfibers from polymeric solutions in the presence of an electric field (Kumar et al., 2022). A standard electrospinning setup consists of a grounded collector, a high voltage power supply, a syringe pump, a metallic needle, and a spinneret (Senthamizhan et al., 2017; Villarreal-Gómez, Cornejo-Bravo, Vera-Graziano, & Grande, 2016). A polymeric solution is injected through a conductive needle onto which a high voltage has been applied, causing the viscous solution to flow toward a grounded collection surface. The polymeric jet experiences solvent evaporation, as well as bending instabilities and long, continuous fibers, oriented randomly or aligned, depending on the collector modality (Chun et al., 2018). The fundamentals of electrospinning have been known for a long time, and the effects of various processing parameters on the morphology of the fibers have been extensively studied (Kumar et al., 2022).

The biomedical sector particularly benefits from ES for the development of advanced systems that are relevant to tissue engineering, drug delivery, wound dressing, and antimicrobial applications (Senthamizhan et al., 2017). Electrospinning offers the potential to produce scaffolds with bioactive compositions and long-term drug delivery capabilities due to their high surface area and interconnected pores (Villarreal-Gómez et al., 2016). Furthermore, the rate of drug release can be tailored by adjusting the fiber diameter, porosity, and drug-binding mechanism of the electrospun nanofibers. Nano- and micro-sized carriers, such as nanoparticles, nanotubes, microspheres micelles, and liposomes can be incorporated into nanofibers as a promising approach for controlled drug delivery (Senthamizhan et al., 2017; J. dos Santos et al., 2021; Banche-Niclot et al., 2022; El-Fiqi, Kim, & Kim, 2015; Lim, Kathuria, Tan, & Kang, 2018; Patel & Yadav, 2018; Torres-Martinez et al., 2019).

The use of nanoparticles (NPs) has been explored as a promising approach of drug delivery systems, due to their nano size, surface properties and their ability to act as vehicles in the transport and delivery of a wide class of drugs and/or proteins, increasing their solubility and bioavailability (Kamsani, Haris, Pandey, Taher, & Rullah, 2021). NPs with drug-functionalized surfaces can modulate drug release by controlling their size, shape, chemistry, and crosslinking, while the nanofibers can provide mechanical stability and the ability to support tissue growth. These NPs can be composed of synthetic polymers such as polylactic acid (PLA), poly lactic-*co*-glycolic acid (PLGA), or polyethylene glycol (PEG) (Rouhollahi, Hosseini, Alihosseini, Allafchian, & Haghighat, 2018). Drug-loaded nanofibers have been demonstrated feasible in several studies **(Table 1.2)**.

3D printed scaffolds could also be employed as drug reservoirs. In the study of Auriemma et al. (2022), the authors mentioned that the interest in three-dimensional (3D) printing in the scientific world, and particularly in pharmaceutical and medical research, has grown exponentially. In fact, the number of scientific papers recorded containing the term "3D printing" increased from 57 in 2012 to 4623 in 2021. In that regard, it is important to continuously strengthen the alliance between AM and nanotechnology to create innovative and multifunctional scaffolds. New methodologies for drug delivery systems with geometric characteristics adapted to overcome problems such as uncontrolled drug release,

uncontrolled biodistribution, and untargeted manner could be developed (Jammalamadaka & Tappa, 2018; Kondiah, Kondiah, Choonara, Marimuthu, & Pillay, 2020; Stewart et al., 2020; J. dos Santos et al., 2021). Drug-loaded nanoparticles have been incorporated into tridimensional scaffolds by using techniques such as bioprinting and SLA. **Table 1.3** summarizes related works on 3D scaffolds containing nano-sized structures for drug delivery applications.

### 1.2.2 The use of polymeric materials for biomedical applications

Polymers have several properties that influence host tissue reaction to implant materials. Chemical composition, structure, morphology, hydrophilicity/hydrophobicity, average molecular weight, mechanism of degradation, and biocompatibility are some of these properties. The ideal biodegradable polymer should produce nontoxic degradation chemical compounds that are easily metabolized and eliminated from the body.

#### Polyvinyl alcohol (PVA)

PVA is one of the most interesting synthetic polymers that has a very high potential in diverse TE and RM applications due to their properties such as non-toxic, non-carcinogenic, bioadhesive, biodegradable, biocompatible, mechanical performance, chemical resistance, and most importantly, the ability to dissolve in aqueous solutions (Bootdee & Nithitanakul, 2021). PVA is a synthetic polymer obtained by the hydrolysis of poly (vinyl acetate). Depending on the proportions of acetate groups in the main chain, PVA can be classified as fully- or partially-hydrolyzed (Mayilswamy, Prakash, & Kandasubramanian, 2022; Torres-Martinez et al., 2019). PVA-based nanofibrous scaffolds have shown great potential in numerous TE applications, including bone, cartilage, skin, vascular, neural, corneal, and as vehicles for the controlled delivery of drugs, proteins, growth factors, etc (Teixeira, Amorim, & Felgueiras, 2020; Torres-Martínez et al., 2020). Blends of PVA with compounds from natural resources is one of the most effective methods for the preparation of composites with specific properties.

#### Poly lactic-*co*-glycolic acid (PLGA)

PLGA is a copolymer formed from polylactic acid (PLA) and polyglycolic acid (PGA) that are connected by ester linkages (Sequeira, Pereira, Ribeiro, Veiga, & Santos, 2020; Xu, 2012). PLGA is relatively hydrophobic, requiring organic solvents for dissolving it. Lactide-rich PLGA copolymers absorb less water and degrade more slowly. Due to their excellent mechanical performance, nontoxic degrading products, biodegradability, biocompatibility, and favorable release kinetics, PLGA has shown immense potential in the production of various therapeutic devices including drug delivery carriers, scaffolds for tissue engineering, surgical sutures, and tissue grafts (Böhm, Tandon, Hrynevich, Teßmar, & Dalton, 2022; Sun, Xu, Wu, Ye, & Wang, 2017; Zhao et al., 2016; Vázquez et al., 2019). Different studies have demonstrated the efficacy of PLGA-based nanoparticles as carriers for encapsulating and delivering hydrophobic agents (Banche-Niclot et al., 2022; Ghosh et al., 2021; Ruiz-Esparza et al., 2014). PLGA nanospheres loaded with protein drugs were incorporated into poly(vinyl alcohol)/Aloe vera (PVA/AV) nanofibers as a novel wound dressing by (Bootdee & Nithitanakul, 2021). The influence of AV and PLGA nanospheres on the physical characteristics, antibacterial activity, and drug release behavior of the composite nanofibers was studied. The results showed how PLGA NPs can increase the

stability of biomolecules, protecting them from enzymatic degradation, and restoring a therapeutic effect within the appropriate therapeutic duration, biodistribution, and concentration (Banche-Niclot et al., 2022). In general, the release of bioactive molecules from biodegradable nanocarriers is regulated by diffusion throughout the polymer matrix, followed by the bulk erosion of the material.

The most common technique used for the preparation of PLGA nanoparticles is the emulsification-solvent evaporation technique. This technique allows the encapsulation of hydrophobic drugs by dissolving the polymer and the compound in an organic solvent. The emulsion oil (O) in water (W) i.e O/W is prepared by adding water and a surfactant to the polymer solution. Through hydrophobic interactions, surface adsorption of surfactants enhances the suspension stability of nanoparticles by ensuring repulsion between them and, thus, minimizing aggregation. PVA is the most commonly used surfactant. The nanosized droplets are induced by sonication or homogenization. The solvent is then evaporated or extracted and the nanoparticles are collected after centrifugation. Drug loading into nanoparticles is achieved by two methods: (i) the incorporation of the drug during the nanoparticles production, and (ii) the adsorption of the drug on nanoparticles after their production (Danhier et al., 2012; Sequeira et al., 2020; Keloglu, Verrier, Trimaille, & Sohier, 2016).

### Polylactic acid (PLA)

PLA is a conventional thermoplastic polymer from the polyester family that is environmentally friendly and approved for use in clinical medicine by the US Food and Drug Administration (FDA). The polymerization of lactic acid generates PLA, which can be derived from renewable sources, such as starch and sugar. Due to the chiral nature of lactic acid, several distinct types of PLA exist, such as poly-L-lactic acid (PLLA) and poly-D-lactic acid (PDLA), which are obtained from polymerizing L-lactic acid and D-lactic acid, respectively, and poly (dl-lactic acid) copolymer (PDLLA) (Turnbull et al., 2018). In the human body, the PLA degradation is by the hydrolisis of the ester-bond backbone. Briefly, water molecules attack the ester bonds of PLA molecules, breaking them into smaller chains. PLA is degraded into water-soluble monomers and oligomers during hydrolysis, which is later decomposed into water and carbon dioxide, and then excreted. The characteristics of PLA (such as crystallinity, molecular weight, etc.) and the conditions of hydrolysis (such as pH, temperature, etc.) play a significant role in this process (Puppi & Chiellini, 2020). Due to its biocompatibility, biodegradability, and processability, PLA has been used to manufacture a wide variety of medical implants, including bone screws, fixation devices, and vascular grafts. For example, highly crystalline. For example, highly crystalline PLAs are among the most employed materials in FDM thanks to their low $T_m$ (<180°C) enabling their processing (Puppi & Chiellini, 2020). Research mentioned above have shown that the fabrication of PLA composite scaffolds by combining manufacturing technologies has a promising future in tissue engineering and drug delivery. It means that PLA can continue to improve its biofunctionality and chemical properties as well as its potential to produce high-performance biomaterials.

### 1.2.3 Hop Extracts

A plant-derived compound obtained from the hop plant *Humulus Lupulus* L; is the Xanthohumol (XN) (R= $C_{21}H_{22}O_5$), the most important flavonoid in hops (Qiao et al., 2016). This metabolite has received growing attention due to its wide spectrum of biological activities and the beneficial effect on human health. For example, has been proven to enhance osteoblast differentiation and proliferation (Jeong et al., 2011). Also, xanthohumol inhibits tumor growth and angiogenesis, and it has demostrated to possess antimicrobial properties. However, an efficient delivery system of XN remains to be searched (Fonseca et al., 2021; Ghosh et al., 2021).

The extract used in this research is a purified, commercial $CO_2$-prepared hop extract obtained from Hopsteiner Company (New York, NY, USA). It contains mainly $\alpha$-bitter acids (humulone R= $CH_2CH(CH_3)_2$), $\beta$-bitter acids (lupulone R= $CH_2CH(CH_3)_2$), and xanthohumol. The **Table 1.4** and **1.5** show a summary of research studies made on activity of xanthohumol and encapsulation methods, respectively.

Therefore, it is necessary to develop multifunctional scaffolds that combine tailored drug delivery systems with specific geometric properties (and that allow to overcome problems such as uncontrolled drug release, uncontrolled biodistribution, and untargeted manner) to overcome the limitations of current systems. In this work, bimodal scaffolds were generated through the combination of FDM and ES, which has been focused on the validation of PVA electrospun fibers loaded with PLGA/XN nanoparticles to promote adequate strength and stiffness during the regeneration process of damaged tissue, as well as facilitate the drug delivery to ensure a rapid and efficient regeneration process *in situ*.

Table 1.1: A review of research studies on bimodal scaffolds produced by electrospinning and additive manufacturing.

| **Technique** | **Based material** | **Fiber material** | **Results** | **Reference** |
|---|---|---|---|---|
| FDM | PCL | PCL | Improvement in cell proliferation, migration, and adhesion | (Huang et al., 2020) |
| FDM | PCL | PCL | Improvement in cell proliferation, migration, and adhesion | (Vyas et al., 2020) |
| FDM | PLA filament | PCL | Improvement in mechanical properties | (Lara-Padilla et al., 2017) |
| Bio-extrusion | PCL | PLGA | Improvement in cell viability and adhesion | (Mota et al., 2011) |
| FDM | PLA | PVA-nHA* | Improved cell adhesion, proliferation and biocompatibility | (Saniei & Mousavi, 2020) |
| FDM | PLLA | Gelatin solution with osteogenon drug | Improved cell adhesion and proliferation | (Rajzer et al., 2018) |
| FDM | PLA filament | PCL | Enhanced biocompatible and biodegradable properties in scaffolds | (Mendoza-Buenrostro et al., 2015) |
| FDM | PLA | Gelatin-forsterite | Improved mechanical and biological properties | (Naghieh et al., 2017) |

*nHA, nanoHydroxyapatite

Table 1.2: A review of research studies on composite nanofibrous scaffolds for drug delivery and tissue engineering applications.

| **Composite Scaffolds** | **Materials** | **Technique** | **Drugs** | **Application** | **Reference** |
|---|---|---|---|---|---|
| Drug-loaded mBGn within the fiber matrix | Bioactive glass, PCL, Gelatin | Electrospinning | DEX | Bone Regeneration | (El-Fiqi et al., 2015) |
| Drug-loaded PLA NPs on PLGA microfibers | PLA, PLGA | Jet-Spraying Co-projection | LZ | Tissue Repair | (Keloglu et al., 2016) |
| CsA-loaded PLGA NPs into PCL-based scaffolds | PLGA, PCL | Electrospinning | CsA | Dental Engineering (Tooth innervation) | (Kuchler-Bopp et al., 2017) |
| MX-Loaded PLGA NPs into Silica-base scaffolds | PLGA, Silica | Electrospinning Sol-Gel | MX | Periodontal Regeneration | (Pouroutzidou et al., 2022) |
| GS-loaded Mesoporous Silica NP into PLGA/PLA based scaffolds | PLGA, Chitosan | Electrospinning | GS | Prevention management of bone infections | (Batista et al., 2022) |
| SDF-1$\alpha$ loaded PLGA NPs into Chitosan-based scaffolds | PLGA, Chitosan | Electrospinning | SDF-1$\alpha$ | Cancer treatment | (Molina-Peña et al., 2021) |
| BSA-loaded PLGA NPs onto PCL-based scaffolds | PLGA, PCL | Electrospraying Electrospinning | BSA | Tissue Engineering | (Shaw & Samavedi, 2021) |

DEX, Dexamethasone; LZ, Lysozyme; CsA, Cyclosporine; MX, Moxifloxacin; GS, Gentamicin Sulfate; SDF-1$\alpha$, stromal cell-derived factor-1$\alpha$; BSA, Bovine serum albumin

Table 1.3: 3D printing scaffolds for drug delivery and tissue engineering applications.

| **AM technique** | **Materials** | **Nanostructure** | **Drugs** | **Application** | **Reference** |
|---|---|---|---|---|---|
| Bioprinting | Type I Collagen | PLGA NPs | TGF-$\beta$1 | Bone Regeneration | (Banche-Niclot et al., 2022) |
| FDM | PLA | PLGA nanofibers | VC, CTZ | Infections prophylaxis during treating the comminuted metaphyseal fracture | (Chou et al., 2017) |
| SLA | PEG, PEGDA | PLGA core-shell nanoparticles | Nerve growth factor | Nerve regeneration | (Lee et al., 2017) |
| nd | PCL, PLLA | Silica NPs | Enrofloxacin | Antibacterial and bone tissue engineering | (Yang, Hu, Wang, & Binks, 2017) |
| nd | HA | PLGA NPs | BMP-2 | Bone tissue engineering | (Kim, Yang, & Kim, 2018) |
| FDM | PEG, PLA | nHA | DEX | Bone Regeneration | (Li et al., 2018) |
| FDM | PVP | PVP nanofibers | Loratadine | Effects of drug-loaded nano-fibers on the solubility of the poorly water-soluble drug | (Ambrus et al., 2019) |
| SSE | PCL | nHA, Silica NPs | Ibuprofen | To fabricate porous scaffolds for bone tissue engineering applications | (Hu et al., 2019) |
| FDM | PLA | Citrate, nHA | Minocycline | Bone regeneration | (Martin et al., 2019) |
| FDM | PCL | Porous silicon nanostructure | BMP | Osteoinductive implants | (Rosenberg et al., 2019) |

TGF-$\beta$1, Transforming growth factor $\beta$1; VC, Vancomycin; CTZ, Ceftazidime; BMP-2, Bone morphogenetic protein 2.

Table 1.4: References on studies on Xanthohumol activity.

| **Dose ($\mu$M)** | **Cell line** | **Results** | **Reference** |
|---|---|---|---|
| 5 to 60 | C6 | XN significantly inhibited the C6 glioma cell proliferation | (Hou, Song, Sun, Zhu, & Wang, 2021) |
| 0-50 | HL-60 Leukemia cells | XN dose-dependently decreased cell viability | (Mi et al., 2017) |
| 5 | HCC | Decreased the cell viability, confluency ability and colony forming | (Kunnimalaiyaan, Sokolowski, Balamurugan, Gamblin, & Kunnimalaiyaan, 2015) |
| 25 | HCC | Suppressed proliferation and migration of HCC. Concentrations up to 100$\mu$M did not affect viability of primary human hepatocytes in vitro | (Hellerbrand, 2009) |
| 10 | HepG2 | No cytotoxic | (Plazar, Žegura, Lah, & Filipič, 2007) |
| 0.01, 0.1, 1 ($\mu$g/mL) | MC3T3-E1 | Treatment of MC3T3-E1 cell with XN resulted in increased expression of RUNX2 | (Jeong et al., 2011) |

Table 1.5: References on studies on Xanthohumol encapsulation

| **Materials** | **Method** | **Objective** | **Concentration** | **Cell line** | **Results** | **Reference** |
|---|---|---|---|---|---|---|
| PLGA/XN, PEO/Resveratrol (RES) | Coaxial Electrospinning | To evaluate the effect of drug content on a new core/shell fiber mesh containing RES and XN | 10/90 XN/PLGA; 20/80, 50/50, 80/20 RES/PEO | MCF-7 cell | Good inhibition effect on the proliferation of breast cancer cells | (X. Zhang et al., 2020) |
| Chitosan, Lupolone (L), XN | Chitosan-based nanocomposites encapsulating L and XN | Measure antimicrobial activity | - | - | Increased antimicrobial effect | (Leonida et al., 2018) |
| PLGA/XN, HA-g-PLLA | Electrospinning | To evaluate the effect of blending HA-g-PLLA | 10wt% XN/PLGA; 10 wt% XN/PLGA-5wt% HA-g-PLLA | MC3TE-E1 | Exhibited one-level toxicity, Good cytocompatibility | (Qiao et al., 2016) |

## 1.3 Hypothesis

It is possible to develop bimodal scaffolds, composed of PVA electrospun meshes loaded with PLGA nanoparticles that release therapeutic natural agents, for its potential application in tissue engineering.

## 1.4 Objectives

### 1.4.1 General

To manufacture and characterize PVA electrospun nanofibers with PLGA/XN nanoparticles incorporated into the nanofibers, and to integrate these meshes into PLA bimodal scaffolds by the combination of electrospinning and fused deposition modeling, as a promising bimodal scaffold for biomedical applications.

### 1.4.2 Specifics

*For the manufacturing process:*

- To determine and validate the optimal parameters for the fabrication of PVA electrospun nanofibers.
- To validate the optimal parameters for the the production of PLGA/XN nanoparticles.
- To validate the incorporation of PLGA/XN nanoparticles into the PVA electrospun nanofibers.
- To validate the fabrication of PLA bimodal scaffolds with embedded PVA/PLGA-XN meshes.

*For the physical and chemical characterization:*

- To characterize the morphology of PVA electrospun nanofibers, PLGA nanoparticles, and the bimodal scaffolds by means of scanning electron microscopy (SEM).
- To determine the size distribution of the nanoparticles by dynamic light scattering (DLS), and to measure the nanoparticles surface charge through Zeta Potential.
- To characterize chemically the materials employed.

*For the biological characterization:*

- To study the cell viability of the bimodal scaffolds *in vitro*

# Chapter 2

# Materials and Methods

## 2.1 Polymers

For the synthesis of nanoparticles, poly(D-L-lactide-*co*-glycolide) (PLGA; 65:35), with an inherent viscosity range of 0.55-0.75 dL/g was purchased from LACTEL (Birmingham, AL; USA). The acetone ($(CH_3)_2CO$) acquired from CTR Scientific (Monterrey, NL; Mexico) was used to dissolve the PLGA. Poly (vinyl alcohol)(PVA, Mw = 89000-90000 and 99+% hydrolyzed) was purchased from Sigma-Aldrich (St. Louis, MO, USA) and used to fabricate the electrospun nanofibers. For the printing of the scaffolds, a commercial 3D filament based on polylactic acid (PLA) (eSUN, Hong Kong SAR, China) of 1.75 mm diameter with a melting temperature of 180°C, a nominal density of 1.240 g/cm$^3$ and a glass transition temperature of 60°C was used.

## 2.2 Xanthohumol Extraction

The extract used in this research was a purified, commercial $CO_2$-prepared hop extract (Hopsteiner) containing mainly $\alpha$-bitter acids (humulone R= $CH_2CH(CH_3)_2$), $\beta$-bitter acids (lupulone R= $CH_2CH(CH_3)_2$), and xanthohumol.

The xanthohumol (XN) extraction was developed by Javier Oswaldo Vázquez Armendáriz during his master thesis. Briefly, the XN was extracted organically from the commercial hop extract by using 50 mL of methanol ($CH_3OH$) provided by CTR (Monterrey, NL; Mexico). For the efficient and gentle elimination of the solvent, a Buchi Rotavapor R100 V (Flawil, Switzerland) was used. The extract was submitted to the evaporation of the solvent at 60°C and 120 rpm for 1 hour until the pure xanthohumol was obtanied. The compound was then transferred to a SCIENTZ-10N lyophilizer (Zhejiang, China) and lyophilized for three days at -85 °C, and a 0.015 bar pressure. After this process, the crystals were crushed by using a single mortar and pestle and turned into a fine powder. The lyophilized extract was then stored under vacuum at -20°C and kept in refrigeration.

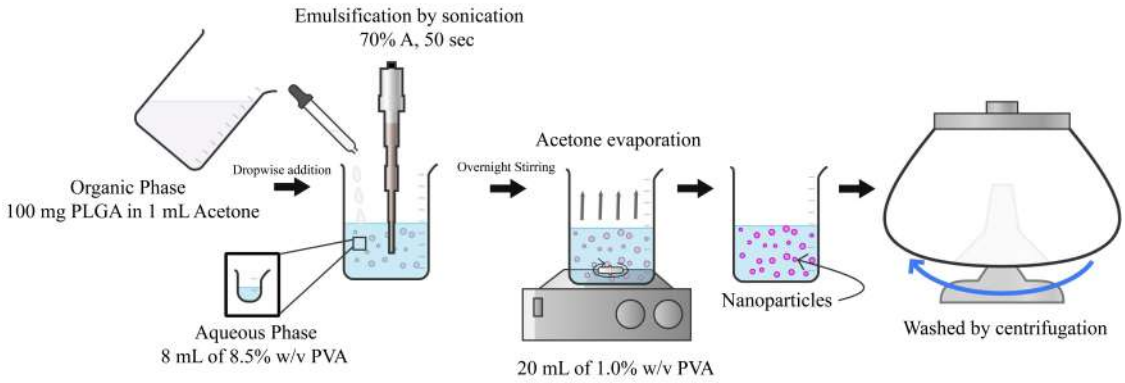


Figure 2.1: Experimental procedure described for production of PLGA nanoparticles.

## 2.3 Manufacturing Process

### 2.3.1 Synthesis of XN-Loaded PLGA Nanoparticles

The PLGA nanoparticles were prepared by a single emulsion method followed by solvent evaporation as described in **Figure 2.1**. Briefly, an aqueous solution of 8 mL of PVA 8.5% (w/v) was sonicated using a QSonica Q500 sonicator (New York, USA) at 70% of amplitude for 50 seconds. An organic phase, prepared with 100 mg of PLGA dissolved in 1 mL of acetone was added dropwise to the aqueous phase during the sonication process to prepare an oil/water (O/W) emulsion. For the evaporation of acetone and precipitation of nanoparticles, the final emulsion was poured to 20 mL of PVA 1% (w/v) under magnetic stirring for 1 day. A centrifuge Eppendorf 5804 (Hamburg, Germany) was used to wash the nanoparticles at 14,000 rpm, 25°C, for 10 minutes. After removing the supernatant, the pellets were resuspended in distilled water, and placed in an ultrasonic bath for approximately 3 minutes, followed by a second wash. A four-step process was used to remove the majority amount of residue from PVA.

The method of preparing the PLGA nanoparticles containing the XN was carried out by using the procedure outlined above with the only difference being that 10 mg of XN was added in the organic phase.

### 2.3.2 Fabrication of PVA Electrospun Nanofibers

For the preparation of the nanofibers, the PVA was dissolved in distilled water at 80 °C with gentle stirring for 3 h to obtain a homogeneous solution at a concentration of 8.5% w/v. The electrospinning set-up is shown in **Figure 2.2**. It consists of a syringe pump Model KS 100 (KD Scientific Inc., Holliston, MA), a power supply (ES20P-5W, Gamma High Voltage Research Inc., Ormond Beach, Florida, USA) and two electrodes, one connected to the needle and the other directly to the aluminum collector of 4 $cm^2$. The electrospinning parameters initially used were 0.2 mL/h, 0.6 mL/h, and 1.0 mL/h flow rates, an electrospinning time of 60 minutes, a voltage of 18 kV, and a distance nozzle-collector of 13-14 cm. These tests were conducted in order to determine which parameters would result in thicker meshes. A Zeiss STEREO light microscope (Oberkochen, Germany) was

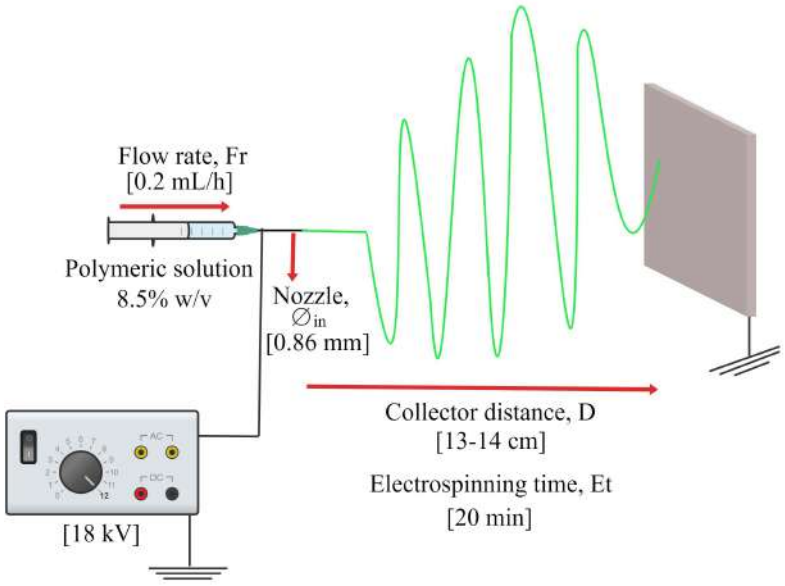


Figure 2.2: Schematic view of electrospinning process.

.

used to measure the mat thickness. Parameters such as temperature, relative humidity, and viscosity were taken into consideration for the fabrication of the electrospun nanofibers.

To measure the mat thickness a section of the mesh was cut out and placed between two microscope slides (**Figure 3.6a**). Eight measurements were performed, in triplicate, for each condition evaluated.

### 2.3.3 Fabrication of the Bimodal Scaffolds

According to the previous protocols used by Lara-Padilla et al. (2017) and Vazquez-Armendariz et al. (2020), the bimodal scaffolds were manufactured in a hybrid printer which was designed and built by Center for Research and Strategic Product Development at Tecnológico de Monterrey. Thermoplastic polymers such as PLA and PCL were used to optimize the parameters. To plot the thermoplastic polymer, a micro extruder with a 0.4 mm diameter nozzle was employed. Layered microfibers were also generated using an integrated electrospinning system. FDM began by placing the thermoplastic polymer filament through the feeder mechanism. After melting the polymer in the micro extruder, the thermoplastic strands were plotted and the first two layers are completed (**Figure 2.3a**). Upon completion of the first two layers, the scaffold was transferred to the electrospinning station (**Figure 2.3b**). The process was repeated until obtaining the final structure (**Figure 2.3c**). During the process, two layers of FDM strands and one layer of electrospun fibers were deposited.

A proportional-integral-derivative (PID) control system governed the extrusion temperature, while another regulated the cooling of the printing base and the electrospinning process. Aerotech MP drivers (Pittsburgh, PA, USA) controlled the stepper motors used for X, Y, and Z axis movement.

LabVIEW v2013 (National Instruments, Austin, TX, USA) was used to design the printer control software. SolidWorks was used to design scaffolds in order to obtain points and cartesian coordinates required for G code structuring. This code was introduced in the control program of the printer for subsequent manufacture.

The scaffolds used for the study were fabricated in a square shape of 5x5 $mm^2$, approximately 1 mm as pore size and 0.4-0.5 mm as the layer height. The final design consisted of four layers of FDM strands and one layer of electrospun meshes.

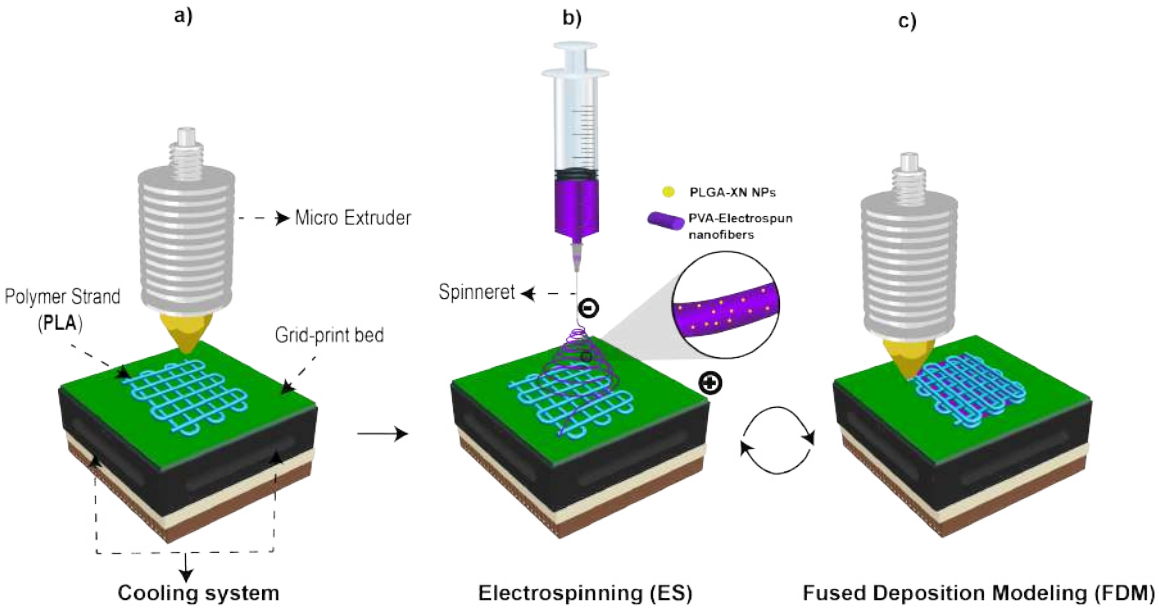


Figure 2.3: Schematic of hybrid processing with Fused Deposition Modeling (FDM) and electrospinning (ESP) with cooling system: (a) initial fused deposition modeling stage; (b) subsequent electrospinning stage; and (c) subsequent fused deposition modeling stage (Lara-Padilla et al, 2017)(Vazquez-Armendariz et al, 2020).

## 2.4 Characterization

### 2.4.1 Characterization of XN-Loaded PLGA Nanoparticles

The particle size distribution and polydispersity index (PDI) of the PLGA and PLGA/XN nanoparticles were analyzed by dynamic light scattering (DLS), by using a Malvern Zetasizer Nano ZS instrument (Malvern Instruments Ltd, Worcestershire, UK). The nanoparticles were previously sonicated to break up agglomerates formed by their interactions. These measurements were conducted in triplicate in clear disposable zeta cells at 25 °C with the following parameters: dispersant viscosity of 0.8872 cP, dispersant refractive index of 1.33, material absorption of 0.010, and material refractive index of 1.59. Zeta potential was determined by electrophoretic mobility analysis with the same equipment. GraphPad Prism was used to process the data collected with the Malvern Zetasizer software. The

morphological features, uniformity of particle-shape and size of PLGA and PLGA/XN nanoparticles were verified by SEM EVOMA25 (Carl Zeiss, Oberkochen, Germany) at an accelerating voltage of 20 kV.

### 2.4.2 Characterization of Electrospun Fibrous Scaffolds

#### Morphology of the electrospun nanofibers

Electrospun nanofiber mats were cut, placed on aluminum stubs, dried overnight in a desiccator, and then coated with a gold film of 5 nm through plasma-assisted sputtering for approximately 15 minutes. The morphology of the samples was analyzed with a Scanning Electron Microscope EVOMA25 (Oberkochen, Germany) at an accelerating voltage of 20 kV. The average diameter of the electrospun nanofibers was calculated from SEM images using ImageJ software. During the measurement process, a total of 70 fibers were selected and analyzed from the SEM micrographs. A histogram of average diameter distribution was plotted by using the collected data.

The distribution of PLGA nanoparticles inside the nanofibers was observed with a Transmission Electron Microscope ARM200F JEOL operated at an accelerating voltage of 200 keV. A sample of the electrospun nanofibers was cut and deposited on a copper TEM grid and covered with carbon. The instrument was equipped with an Energy-Dispersive Spectrum (EDS) to know the crystallinity of the nanofibers.

#### Fluorescence Microscopy

Rhodamine B (Rh), pratical grade, was used to ensure that the NPs were being incorporated into the nanofibers. For the incorporation of Rh, 6 g were dissolved in 40 mL of acetone. A thermo scientific centrifuge was employed to wash this solution at 13,000 rpm, 20°C, and 5 minutes. 1 mL of the supernatant was used to dissolve 100 mg of PLGA and synthesize the NPs as previously described (**Figure 2.1**). Rh-loaded PLGA NPs were dispersed in PVA solution to obtain the meshes. A glass microscope slide was used to collect these meshes. A Zeiss Axio Observer.Z1 microscope (Zeiss, Germany) was employed to observe nanofibers. A 63X objective was applied to all micrographs. LED illuminator intensity and exposure time were 67.3% and 2490 milliseconds (ms), respectively. Before fluorescence analysis, a cover glass was placed over the sample and a drop of immersion oil was deposited. The optical and viscosity characteristics of immersion oils enhance the resolution and brightness of microscope images. Because it reduces light refraction by replacing the air gap between the objective lens and cover glass.

#### Interaction of XN, PLGA NPs and PVA electrospun nanofibers Assessed by Fourier Transform Infrared Spectroscopy with Attenuated Total Reflectance (ATR-FTIR)

Chemical analysis of XN powder, PLGA NPs, and PVA meshes with and without NPs were performed by using a FTIR equipment (Perkin-Elmer Frontier, Mexico City, Mexico) with a universal ATR polarization accessory. The spectra were obtained by collecting 16 scans of each sample, between 4000 and 600 cm$^{-}$1, with a resolution of 4 cm$^{-1}$.

**PVA Electropun Nanofibers Thermogravimetric Analysis (TGA)**

The degradation and thermal stability of PVA meshes were evaluated using a Perkin-Elmer Pyris 8000 TGA analyzer (Mexico City, Mexico). Under a nitrogen atmosphere, samples of approximately 3 mg were heated from 25 to 600 °C at a rate of 10 °C/min.

### 2.4.3 Morphology of the Bimodal Scaffolds

The 3D PLA scaffolds were coated with a gold film of 5 nm through plasma-assisted sputtering for approximately 15 minutes. The morphology of the samples was analyzed with a SEM EVOMA25 (Oberkochen, Germany) at an accelerating voltage of 10 kV. SEM images were used to evaluate the scaffold geometry (pore size, strand diameter, and layer height), and the distribution and incorporation of meshes

## 2.5 Cytotoxicity Assay

To assess the *in vitro* cytotoxicity of the scaffolds, human fibroblasts cells (Detroit 548, CCL-116, American Type Culture Collection, Rockville, MD, USA) were seeded ($4x10^3$/well) with 200 $\mu$L of Dulbecco's Modified Eagle's Medium (DMEM) supplemented with 10% fetal bovine serum (FBS) in 96-well culture plates (Corning®, Cat. No. CLS3596). Cells were allowed to grow for 24 h. Afterward, the medium was changed to 200 $\mu$L of fresh medium and 5 $\mu$L of hop extract (4mg/mL in methanol) was added. Disc samples (5mm) were cut from the meshes. The discs and the 3D scaffolds were placed on top of the monolayer of cells with help of tweezers. The cultured plates were then incubated under an atmosphere of 5% $CO_2$, at 37°C for 24 h. Subsequently, the culture medium was removed and 100 $\mu$L of fresh medium and 10 $\mu$L of MTT (5 mg/mL) (BioBasic, Cat. No. T0793) were added and incubated at 37°C for 4 h.

In *vitro* cell viability was examined by using the MTT assay (Ciapetti, Cenni, Pratelli, & Pizzoferrato, 1993). This method is based on the conversion of MTT (3-(4,5-dimethylthiazol-2yl)-2,5-diphenyltetrazolium bromide) to formazan, which determines mitochondrial activity. After incubation, the medium was removed and 100 $\mu$L of dimethylsulfoxide (DMSO, Fisher, No. Cat. D128-1) was added and mixed until the formazan crystals dissolved and the absorbance at 570 nm was read with a Biotek Synergy 2 plate spectrophotometer (Winooski, VT, USA). Before reading in the spectrophotometer, membranes and 3D constructs were removed.

As a blank, 200 $\mu$L of medium was used per well. The medium with untreated cells was used as negative control, and an additional control with 200 $\mu$L of DMEM/10% FBS and 5$\mu$L of methanol was performed. Cell viability and mortality percentages were calculated according to the following equations (Eskandani et al., 2014):

$$\text{Cell viability } (\%) = \frac{\text{OD of treated cells} - \text{OD of blank}}{\text{OD of untreated cells} - \text{OD of blank}} * 100 \tag{2.1}$$

*OD: Optical density*

$$\text{Mortality}(\%) = 100 - \text{Cell viability } (\%) \tag{2.2}$$

# Chapter 3

# Results and Discussion

## 3.1 Characterization of XN-Loaded PLGA Nanoparticles

In general, DLS is used to determine the particle size distribution of nanosize droplets in polymer emulsions, colloids, suspensions, or solutions. This technique is based on detecting the rate of diffusion of particles, whose Brownian motion is greater the smaller their size, by irradiating the sample with a laser. The particle size distribution as a function of intensity is shown in **Figure 3.1** for PLGA and PLGA/XN nanoparticles. The presence of two distinct populations of particles, smaller (100-1000 nm) and larger (> 1000 nm), can be observed. Through DLS illumination, the particles use the laser to analyze the intensity fluctuations in the scattered light. The laser is sensitive to the presence of large particles/aggregates/dust. This means that larger particles can scatter the laser path more, and generate a certain intensity, as demonstrated in the figures. DLS will not precisely characterize a polydisperse sample.

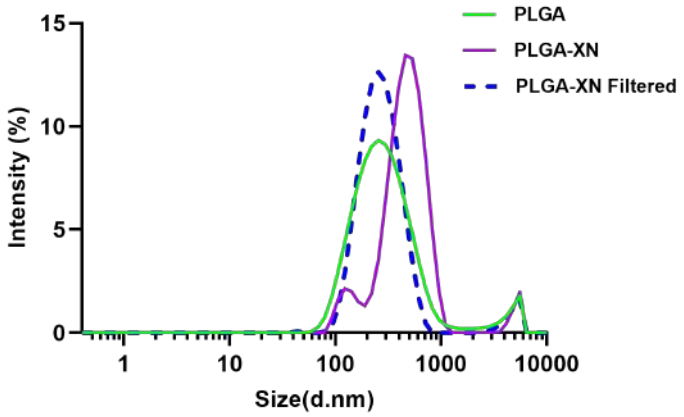


Figure 3.1: PLGA nanoparticle size distribution prior to and after encapsulation with XN.

For PLGA NPs, the average size was 252.93 nm ± 2.08 with a polydispersity index (PDI) of 0.36 ± 0.02. For the PLGA/XN NPs, the average size was 479.15 nm ± 13.36 with a PDI of 0.43 ± 0.06. According to the literature, a PDI between 0.0-1.0 indicates a narrow distribution, 0.1-0.4 moderate and > 0.4 wide. The PDI reported here indicates a moderate size distribution for PLGA NPs and a broad size distribution for PLGA/XN

NPs. As a result of XN presence, the average diameter of NPs increased significantly. It is possible that the formation of larger particles or aggregates occurred during the synthesis process because of electrostatic interactions among particles. In the case of agglomeration, the DLS technique may be unable to accurately determine the Z-average size as it is sensitive to small changes in the sample.

To avoid agglomeration formation and to obtain a smaller size, the PLGA/XN NPs were filtered before washing with a syringe filter (glass fiber membrane of 1 $\mu$m pore size). As can be seen in the **Figure 3.1**, the particle size distribution of the PLGA/XN NPs filtered is more uniform with a value of 261 nm ± 2.51 and a PDI of 0.26 ± 0.01. As noted by Akolpoğlu Başaran, Gündüz, Tezcaner, and Keskin et al. (2021) it is important to obtain smaller and monodisperse NPs to achieve a homogeneous distribution of NPs in the scaffold and for controlled drug release.

The zeta potential is a measure of the particles surface charge. In the case of PLGA NPs is negative due to the carboxyl groups of lactic-*co*-glycolic acid residing on the surface of the particles (Surassmo et al., 2015). In previous studies, zeta potential values of PLGA NPs which were obtained with single emulsion method followed by solvent evaporation were reported as -27.10 mV ± 8.40 and -16,4 mV ± 0,23 (Akolpoğlu Başaran et al., 2021). Other results are summary in **(Table 3.1)**

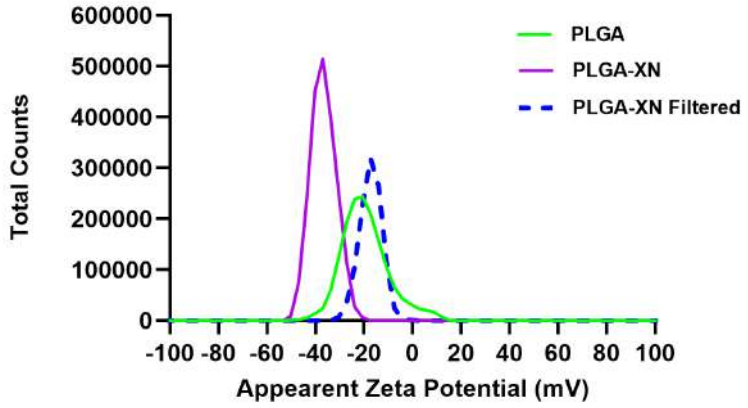


Figure 3.2: Zeta potential analysis of PLGA nanoparticles prior to and after encapsulation with XN.

Table 3.1: References on the characterization of PLGA nanoparticles.

| Reference | NPs | Size [nm] | Zeta Potential [mV] | PDI |
|---|---|---|---|---|
| (Ghosh et al., 2021) | PLGA | 201.9 ± 0.1 | -21.6 ± 0.3 | 0.045 |
| | PLGA-XN | 191.0 ± 0.8 | -24.8 ± 0.2 | 0.029 |
| (Fonseca et al., 2021) | PLGA | 273 ± 18 | -15.4 ± 2.1 | 0.285 |
| | PLGA-XN | 312 ± 49 | -18.2 ± 1.4 | 0.259 |
| (Banche-Niclot et al., 2022) | PLGA/TGF-$\beta$1* | 256.6 ± 7.3 | -33.5 ± 6.0 | 0.1 ± 0.5 |

TGF-$\beta$1*, Transforming growth factor $\beta$1

As shown in **Figure 3.2**, the zeta potential of the PLGA NPs was -19.9 mV ± 0.62, and with the addition of XN was -39 mV ± 1.27. Fonseca et al. 2021, Ghosh et al. and Banche-Niclot et al. 2022 suggest that the more negative potential of loaded PLGA NPs **(Table 3.1)** can be attributed to the exposure on the surface of encapsulated drug. The adsorption process is governed by noncovalent interactions, including electrostatic, hydrophobic, and Van der Waals forces (Chatterjee & Chanda, 2022). According to this, the more negative zeta potential for the PLGA/XN nanoparticles could be since the XN was adsorbed on the surface. However, for the PLGA/XN NPs filtered, the zeta potential decreased to -16.07 mV ± 0.38. Fonseca et al. 2021 and Ghosh et al. 2021 mentioned that small size, unimodal distribution, and negative surface charge result in higher particle-particle repulsion, thus increasing formulation stability. In this case, the filtration was better since smaller particles were obtained and the distribution was more homogeneous. Therefore, the method explained in this work to obtain PLGA/XN NPs is feasible and reproducible. **Table 3.2** presents the nanoparticle characterization results obtained in this work

Table 3.2: Nanoparticle characterization results obtained in this work

| NPs | Size [nm] | Zeta Potential [mV] | PDI |
|---|---|---|---|
| PLGA | 252.93 ± 2.08 | -19.90 ± 0.62 | 0.36 ± 0.02 |
| PLGA-XN | 479.15 ± 13.36 | -39 ± 1.27 | 0.43 ± 0.06 |
| PLGA-XN filtered | 261.23 ± 2.51 | -16.07 ± 0.38 | 0.26 ± 0.01 |

The morphology of PLGA and PLGA/XN particles is shown in **Figure 3.3**. SEM images showed sphere-shaped particles. The presence of large particles, 3 to 6 microns in size, was evident. Also, there were smaller ones, between 500 to 700 nanometers. It was difficult to see smaller particles at a higher magnification because larger particles were affected by the high voltage used during characterization. Agglomeration was observed (dashed red circles) because of the Ostwald Ripening Effect, a general growth mechanism that controls nanoparticle synthesis. This process leads to the diffusion of smaller particles onto bigger ones, increasing particle size. This happens because colloidal particles are inclined to minimize their surface-to-volume ratio, thereby minimizing their surface-free energy. Ostwald ripening occurs when nanoparticles (either organic or inorganic) are dispersed in a solution. Materials such as polymers, metals, and inorganic oxides exhibit this phenomenon (Hernández-Cruz et al., 2016; Piletska et al., 2017; Dagtepe & Chikan, 2010). The morphology of the PLGA/XN particles after filtration is shown in **Figure 3.4**. Some particles are in the range of 100-200 nm in size. In addition, agglomerates decreased evidently. Because of the high acceleration voltage (20 kV) and the higher magnification used during characterization, some nanoparticles acquired an oval shape. Polymeric NPs are sensitive to the high energy of electron beams, which causes them to collapse or erode. When beam energy increases, primary electrons penetrate deeper into solid specimens, affecting surface detail.

These results confirmed that a filtration phase was essential to achieve a better particle size distribution and to prevent the formation of agglomerates and large particles. Since NPs with diameters between 100-200 nm would be optimal for *in vivo* applications (Singh, Tanurajvir, Ravinder, & Kaur, 2014).

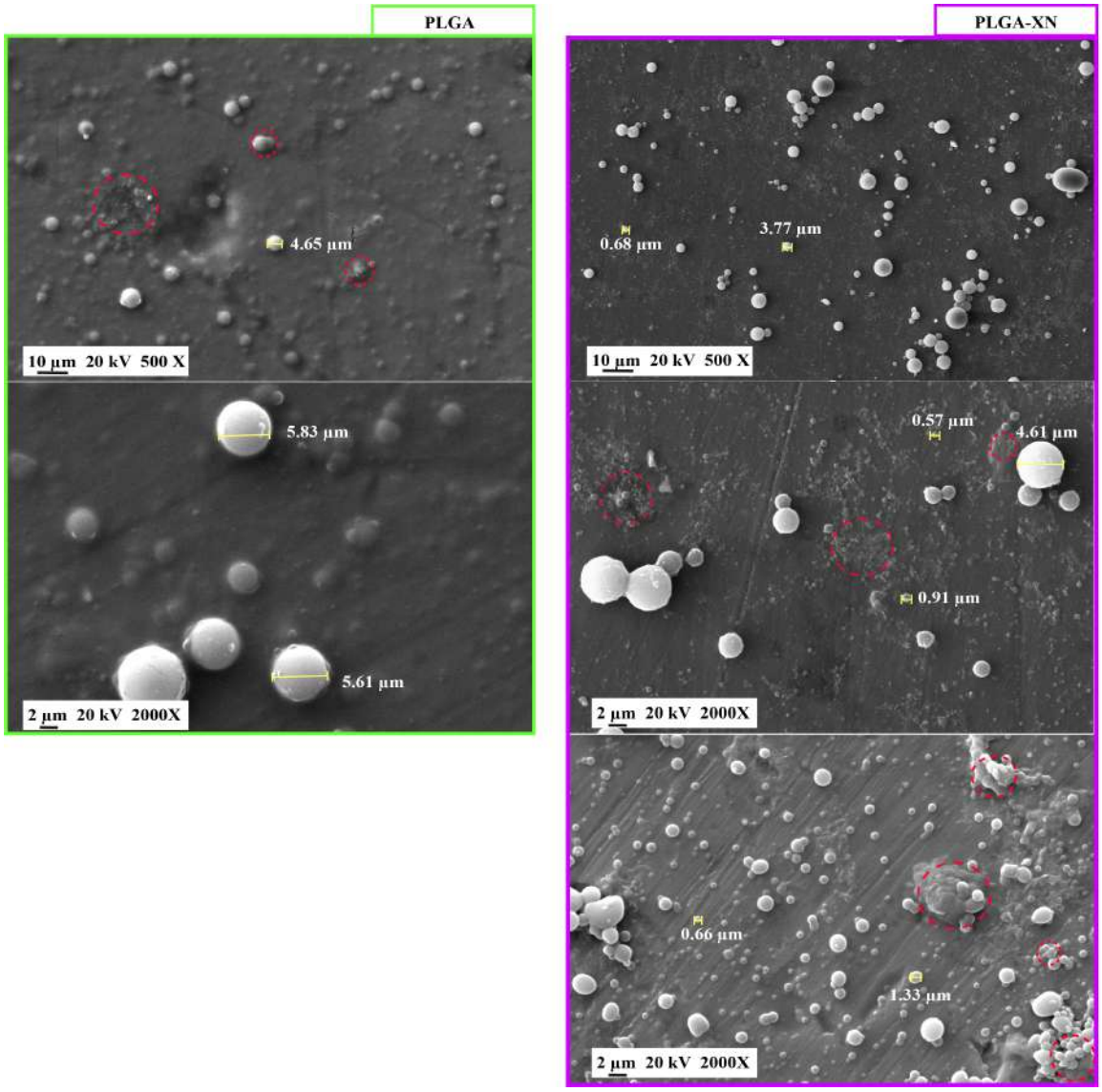


Figure 3.3: SEM images of PLGA and PLGA/XN particles particles.

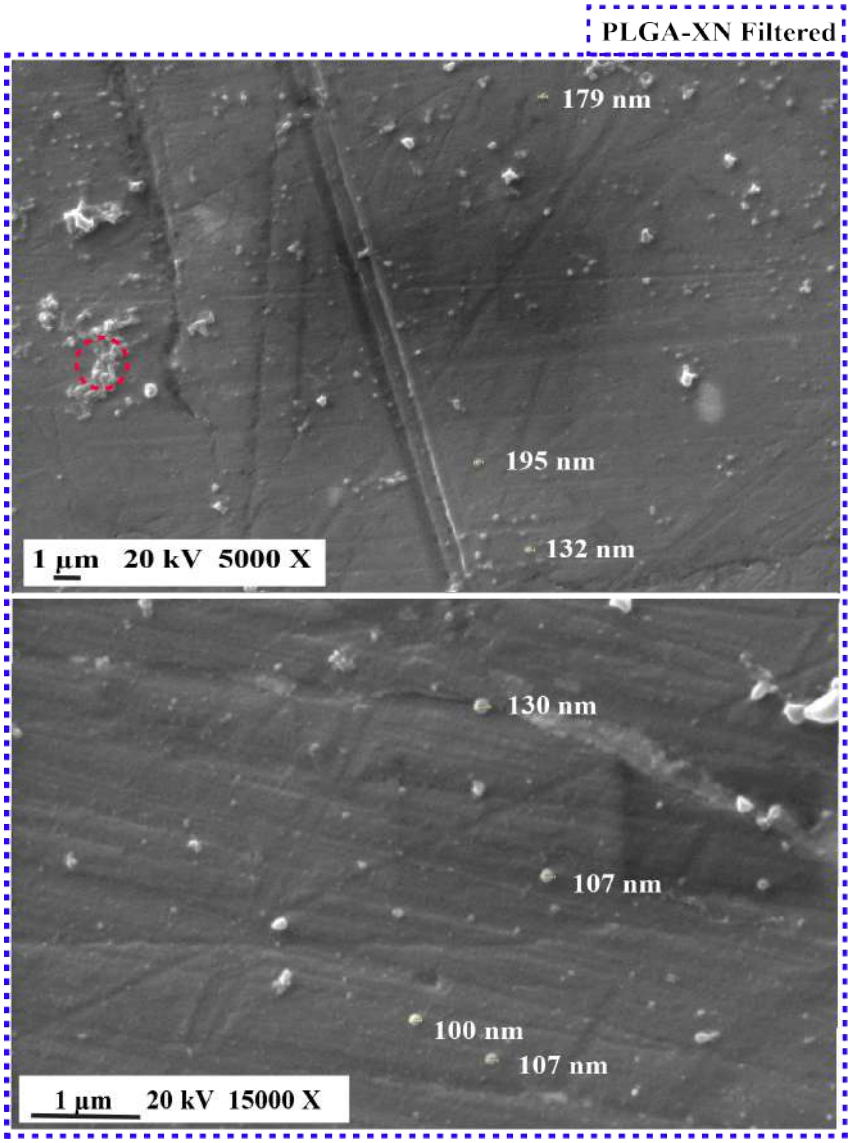


Figure 3.4: SEM images of filtered PLGA/XN Nanoparticles.

## 3.2 Characterization of Electrospun Nanofibrous Scaffolds

### 3.2.1 Morphology of the Electrospun Nanofibers

The initial parameters used in electrospinning are summarized below:

Table 3.3: First electrospinning parameters

| **Parameter** | **Value** |
|---|---|
| Flow rate, $F_r$ [mL/h] | 0.2, 0.6 and 1 |
| Distance nozzle-collector, D [cm] | 13-14 |
| Electrospinning time, $E_t$ [min] | 60 min |
| Applied Voltage, V [kV] | 18 |
| Nozzle Diameter, $\varnothing_{in}$ [mm] | 0.86 |

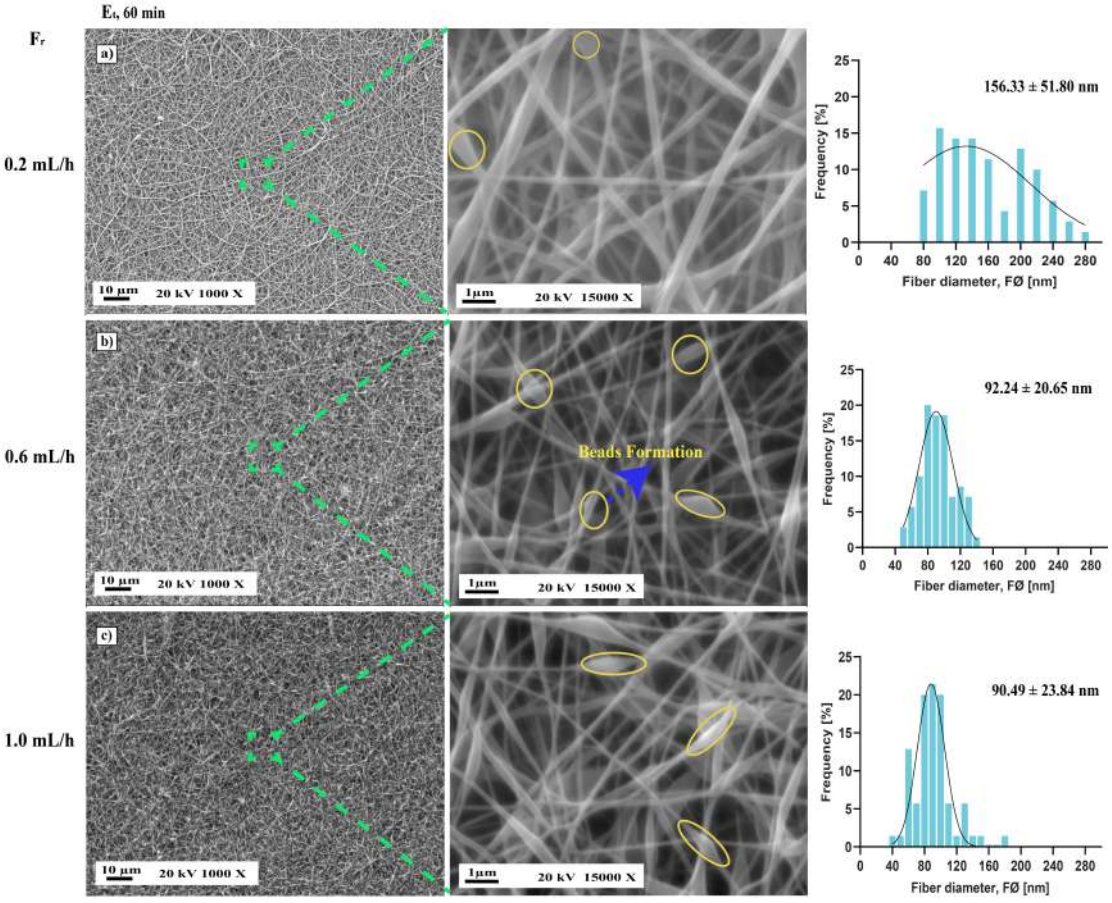


Figure 3.5: Morphology of the PVA electrospun nanofibers.

**Figure 3.5** illustrates the effect of solution flow rate on fiber morphology. With a flow rate of 0.2 mL/h, the jet was more stable and fiber morphology included fewer beads (**Figure 3.5a**). By increasing the flow rate, a major jet distortion was generated, resulting in the formation of beads due to non-evaporation of the solvent and low stretching in the

solution during a flight between the needle and metallic collector as illustrated in **Figure 3.5b-c**. Initially, the objective of this test was to determine the optimal parameters for thicker meshes with defect-free morphology. A thicker mesh will allow more drugs to be loaded. As a result, the mesh degradation time will be longer, prolonging period of time for drug release. The advantage of electrospinning in drug delivery is that drugs can be loaded into the fibers to improve their bioavailability or to achieve controlled release (Torres-Martinez et al., 2019; Torres-Martínez et al., 2020). According to **Figure 3.6b**, mat thickness increased with flow rate at the same electrospinning time (60 minutes). The mat thickness was 5.92 $\mu$m ± 0.75 at 0.2 mL/h, 14,39 $\mu$m ± 1.7 at 0.6 mL/h, and 19.14 $\mu$m ± 2.73 at 1.0 mL/h. These results indicate that flow rate significantly affect mat thickness. However, the optimal parameters that were chosen to obtain PVA electrospun nanofibers with smooth, uniform, and bead-free morphologies were a 0.2 mL/h flow rate, 18 kV voltage, 13-14 cm distance, and an electrospinning time of 20 minutes. The electrospinning time was changed because the hybrid printer employed to manufacture bimodal scaffolds was not isolated from the electric field. Therefore, 60 minutes of electrospinning was considered a long exposure time. In addition, Armendariz in his master's thesis obtained suitable meshes with an electrospinning time of 20 minutes, and the manufacture of bimodal scaffolds was not affected. Although mat thickness decreased at 5.70 $\mu$m ± 3.67 in 20 minutes, a defect-free morphology was obtained as shown in (**Figure 3.7**). This study indicates that the electrospinning time and flow rate significantly affect mat thickness. Further research could be conducted on this topic in the future. For example, for applications in drug delivery systems and the manufacture of bimodal scaffolds.

Environmental factors, such as relative humidity and temperature, also affect the diameter and distribution of the fibers (Sanchez-Alvarado et al., 2018). Relative humidity causes changes in the nanofiber diameter by controlling the solidification process of the charged jet (Torres-Martínez et al., 2020). Due to the high relative humidity, less solvent is evaporated resulting in a reduction in fiber diameter as indicated in the **Figure 3.6c**. PVA average fiber diameters for 60 minutes of electrospinning at 0.2 mL/h, 0.6 mL/h, and 1 mL/h were 156.33 nm ± 51.80, 92.24 nm ± 20.65, and 90.49 nm ± 23.84, respectively. The PVA average fiber diameter for 20 minutes of electrospinning at 0.2 mL/h was 131.45 nm ± 23.47. The fiber diameter distribution is a parameter that is reported when electrospun nanofibers are manufactured. The purpose of this thesis was not to evaluate how the fiber diameter affects the potential application of the scaffolds proposed herein.

PVA electrospun nanofibers morphology with the incorporation of PLGA and PLGA/XN NPs are shown in **Figure 3.8a-b**. The average diameter distribution of the meshes with PLGA and PLGA-XN NPs were 85.46 nm ± 37.84 nm and 112.87 nm ± 49.31, respectively. The addition of NPs not affected fiber formation or integrity, but the presence of beads was evident. The addition of NPs into polymer solution will change the viscosity of the solution, which leads to bead formation during spinning. The SEM images showed the presence of some particles (blue circles) and beads formation. The nanofibers morphology with filtered PLGA/XN NPs showed a more homogeneous distribution of them and fewer beads (**Figure 3.8c**). NPs filtration decreases the number of large particles or aggregates, thereby improving nanofiber morphology. According to Akolpoğlu Başaran et al. et al. (2021), for homogeneous NPs distribution into scaffolds and controlled drug release, small and monodisperse NPs are essential.

Several analyses were considered during this process to evaluate whether NPs was incorporated. In **Figure 3.9**, backscattered electrons (BSE) were used to characterize meshes with PLGA/XN NPs (unfiltered). Based on the composition of the surface, BSE generates images with different levels of brightness. The shades on the grayscale are different if the NPs have a different electronic density than beads and/or fibers. Results show some NPs incorporated, and some large particles on the fiber surface. In addition, beads were evident. **Figure 3.10** shows the morphology of meshes in cross-section. These results also showed the presence of some NPs and the formation of beads. To ensure the incorporation of NPs, TEM and fluorescence microscopy were used to characterize the meshes.

In TEM images, **Figure 3.11 a-b**, beads are highlighted by red ovals, and nanoparticles are highlighted by green ovals. Unlike nanoparticles, beads are composed of the same polymer, so they are lighter. Also, these differences may be due to differences in the molecular weights of the polymers. **Figure 3.11 c-d** indicate that the fibers were amorphous and that the smallest fiber had a diameter of 50 nm.

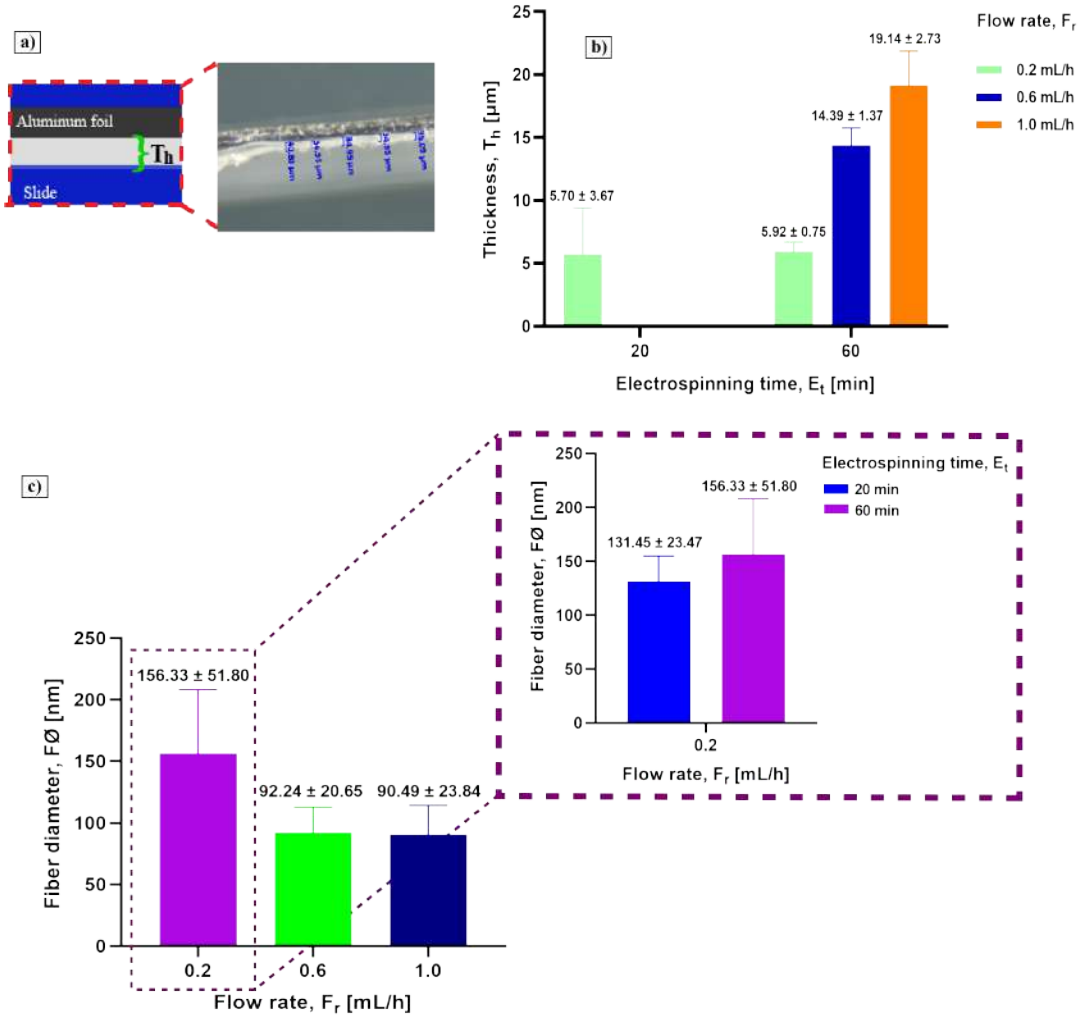


Figure 3.6: (a) Mats thickness measurement scheme; (b) Mats thickness variation with the electrospinning time and flow rate; (c) Fiber diameter variation with the flow rate.

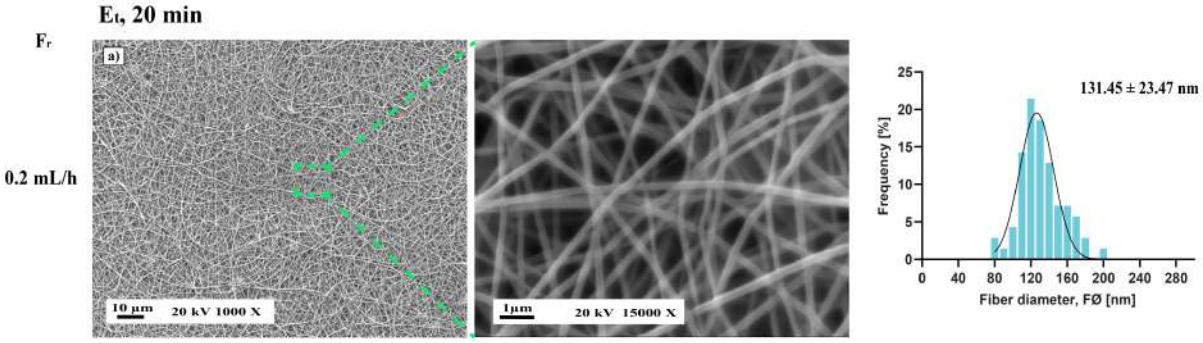


Figure 3.7: Morphology of the PVA electrospun nanofibers with the optimal parameters.

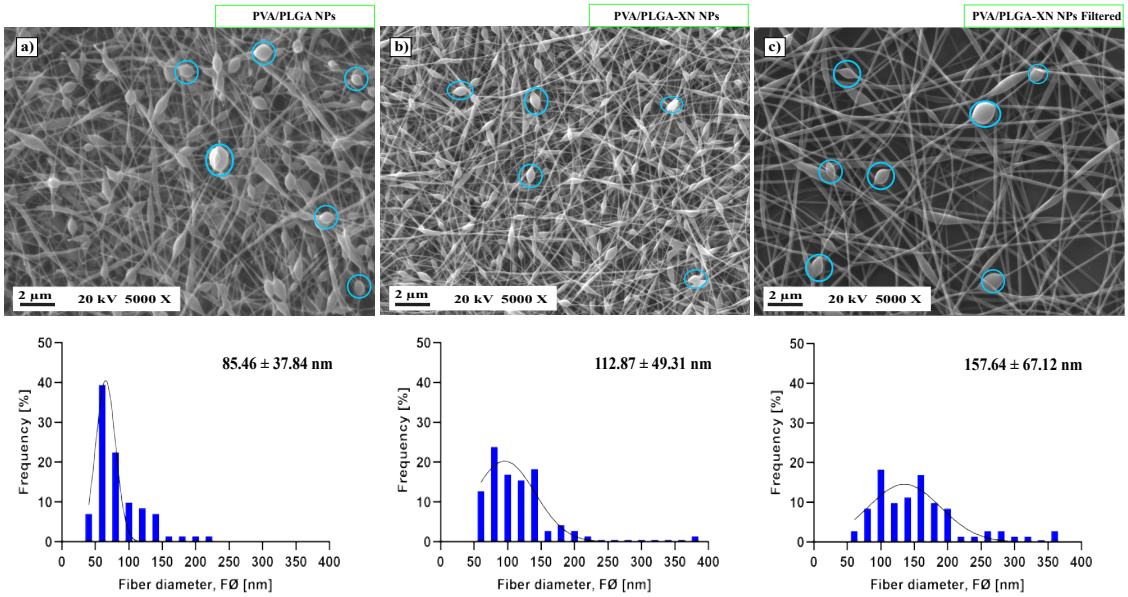


Figure 3.8: Morphology and fiber diameter distribution of the PVA nanofibers with the incorporation of (a) PLGA NPs, (b) PLGA-XN NPs and (c) PLGA-XN NPs filtered.

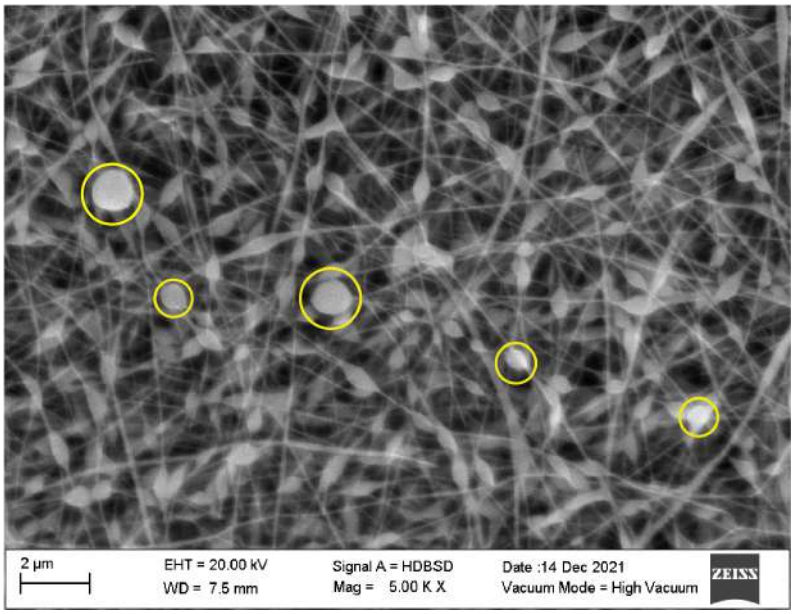


Figure 3.9: SEM image of PVA nanofibers with PLGA/XN NPs using the HD backscattered detector (HDBSD).

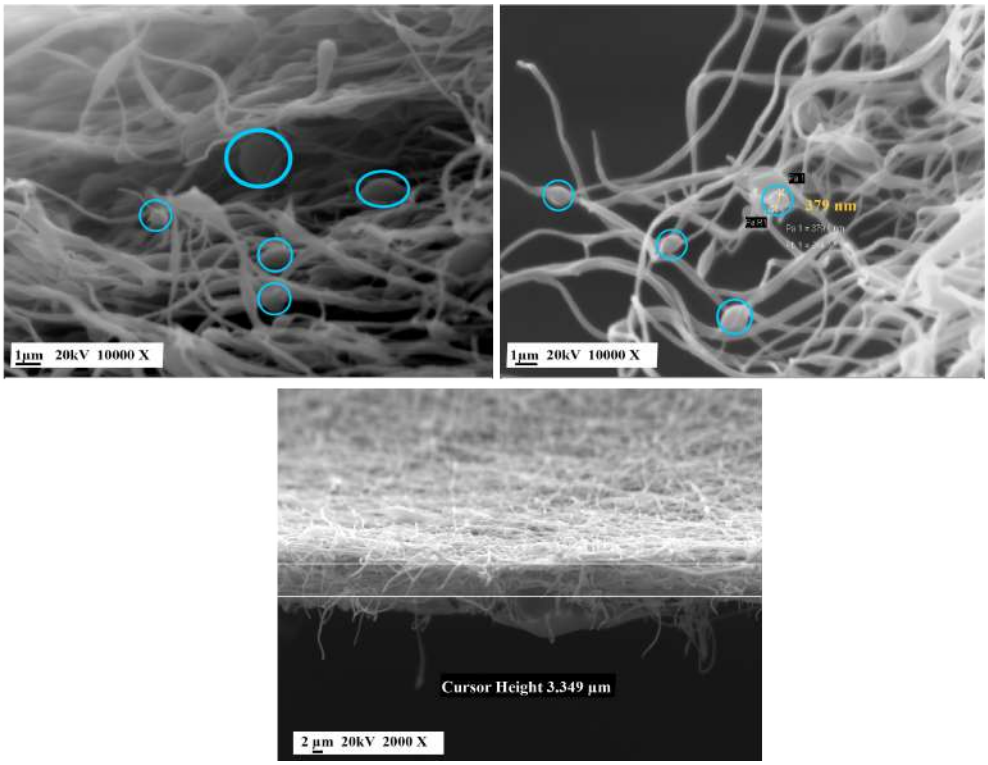


Figure 3.10: SEM image of the cross-section of PVA nanofibers with incorporated PLGA NPs.

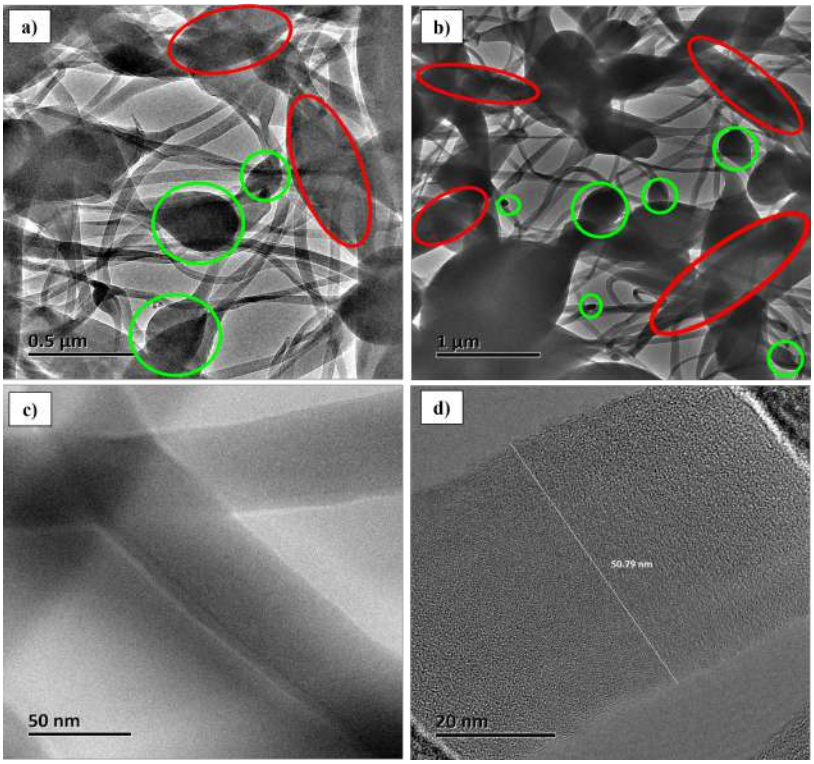


Figure 3.11: TEM images of PVA nanofibers with incorporated PLGA NPs

### 3.2.2 Fluorescence microscopy

Rhodamine B (Rh) was used to ensure that the NPs were being incorporated into the nanofibers. **Figure 3.12** show the brightfield, merged, and fluorescence images of the PVA nanofibers with PLGA NPs empty and loaded with Rhodamine. The PLGA/Rh NPs were integrated into PVA nanofibers as demonstrated by their fluorescence.

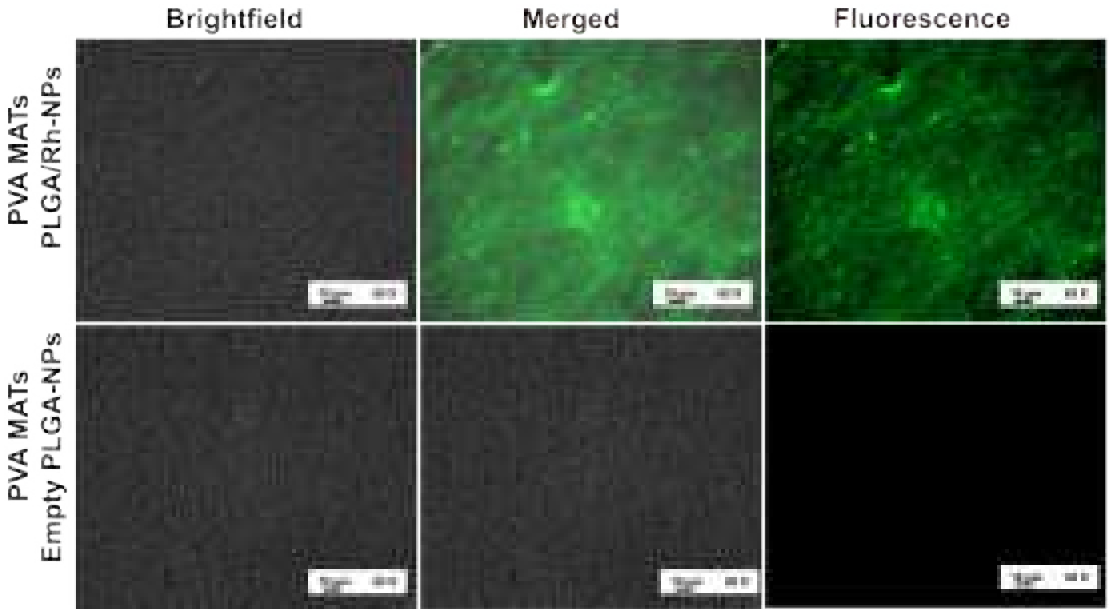


Figure 3.12: Fluorescence microscopy images of PVA electrospun nanofibers with incorporation of PLGA NPs with and without Rhodamine B.

### 3.2.3 Interaction of XN, PLGA NPs, and PVA Electrospun Nanofibers Assessed by ATR-FTIR

Infrared spectroscopy is a characterization technique to enable investigate the structure chemical composition and the bonding arrangement of constituents in polymeric materials (Singh et al., 2014). The ATR-FTIR analysis was conducted to investigate the interactions of PVA electrospun nanofibers with PLGA and PLGA/XN NPs.

PVA mat, PLGA NPs, and XN powder were used as controls. **Table 3.4** summarizes the most characteristic absorption bands and vibrations mode of PVA mat, PLGA NPs, and XN. **Figure 3.13** shows the FTIR spectra to PVA mats, PLGA NPs and XN. PVA mat exhibited a characteristic peak of absorption between 2840-3000 $cm^{-1}$, which is attributed to C–H symmetric stretching vibrations from alkyl groups. C–H bending vibrations occurred at 1416–1328 $cm^{-1}$. C-O stretching vibrations of acetyl groups and C–H rock peaks were identified at 1080 and 844 $cm^{-1}$, respectively (Bootdee & Nithitanakul, 2021). PLGA exhibits C-H stretching and bending vibrations between 2995-2946 $cm^{-1}$ and 1450-850 $cm^{-1}$, respectively. Characteristic signals, between 1750-1763 $cm^{-1}$, are attributed to the stretching vibrations of the C=O groups. Stretching vibrations of the C-O groups between 1187-1188 $cm^{-1}$ were identified (Singh et al., 2014).

PVA mats, PLGA NPs and XN spectrums showed a peak at 3500-3200 $cm^{-1}$ assigned to the O-H stretching vibration of the hydroxyl group. The C=O stretching spectral band at 1600 $cm^{-1}$, and –C=C– vibrations at 1544 $cm^{-1}$ and 1514 $cm^{-1}$, due to phenol and hydroxyl-benzoyl fractions were also observed in the XN spectrum (Fonseca et al., 2021).

The characteristic bands of the PVA mat were more intense and wider in the spectrum of the PVA/PLGA mat. It means that PLGA NPs and PVA exhibited intermolecular interactions. A very faint band characteristic of the C=O group was observed at 1752. In the case of the PVA/PLGA-XN spectrum, it was difficult to distinguish the characteristic bands of PLGA NPs and XN. This is due to the fact that PVA is found in higher concentrations with respect to PLGA-XN NPs. As a result, the signals could overlap.

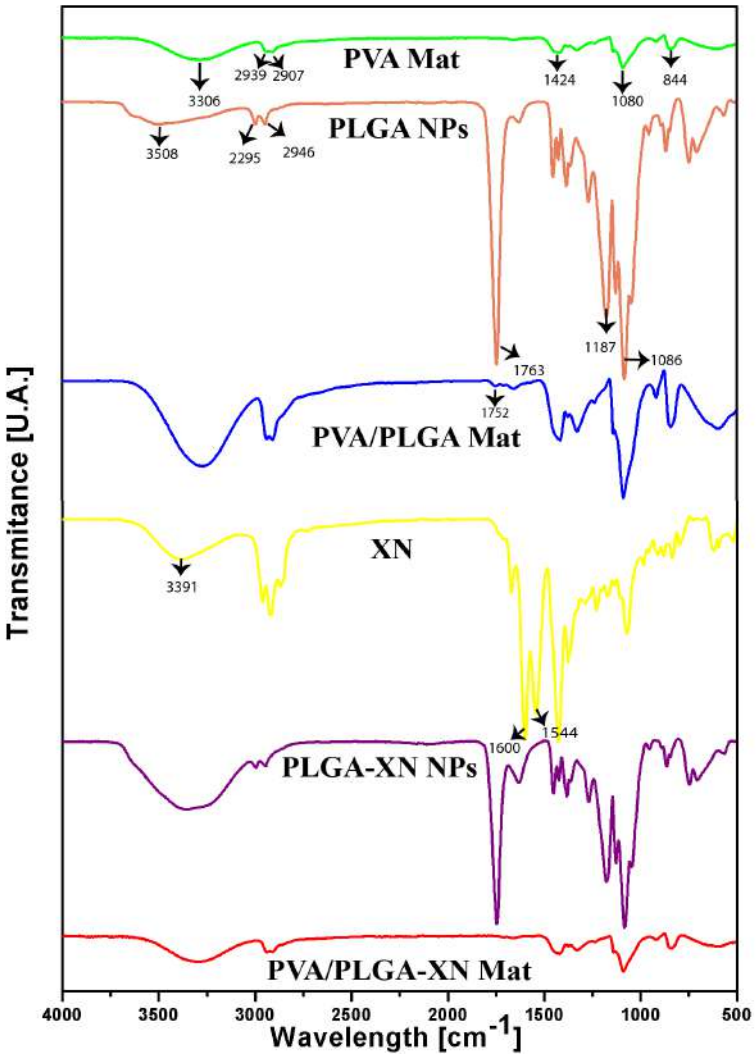


Figure 3.13: ATR-FTIR spectra of PVA, PVA/PLGA, PVA/PLGA-XN mats, PLGA nanoparticles and XN.

Table 3.4: Summary of the most characteristic absorption bands and vibration modes in the ATR-FTIR spectra of PVA mats, PLGA NPs and XN.

| Sample | Assigment bonds | Vibration mode | Peak position [$cm^{-1}$] |
|---|---|---|---|
| PVA Mat | OH | Hydroxyl group | 3500-3200 |
| | C-H | Symetric stretching vibrations from alkyl groups | 2840-3000 |
| | C-H | Bends | 1416-1328 |
| | C-O | Stretching | 1080 |
| | C-H | Rocks peaks | 844 |
| PLGA NPs | OH | Hydroxyl group | 3500-3200 |
| | C-H | Stretching | 2995-2946 |
| | C=O | Stretching | 1763 |
| | C-H | Bends | 1450-850 |
| | C-O | Stretching | 1187-1188 |
| XN | OH | Hydroxyl group | 3500-3200 |
| | C=O | Stretching | 1600 |
| | -C=C- | Hydroxyl-Benzoyl fractions | 1544 |

### 3.2.4 PVA Electrospun Nanofibers Thermogravimetric Analysis

TGA was used to investigate the effect of PLGA and PLGA/XN NPs on the thermal stability of PVA electrospun nanofibers. The stability as a function of temperature-dependent weight changes are shown on the thermograms in **Figure 3.14a**. The corresponding derivative thermogravimetry (DTG) are shown in **Figure 3.14b**, which indicated the temperature at which the maximun weight loss happen.

PVA meshes, with and without NPs, exhibited three distinct stages of weight loss. Approximately 5% of the initial weight loss, below 150 °C, could be due to moisture loss since PVA is a hydrophilic polymer. The second stage, which results in approximately 62-68% weight loss, occurred between 200-400 °C due to the removal of the hydroxyl group and degradation of the PVA backbone. The third step ocurred above 400°C where the decomposition products are carbon and hydrocarbons, produced by the degradation of polyene structures (Torres-Martínez et al., 2020; Park et al., 2019).

Some changes were observed in the PVA meshes due to the incorporation of PLGA and PLGA-XN NPs. The thermogram of the PVA/PLGA mat showed that thermal stability increased with the addition of PLGA NPs. DTG curves indicate the greatest weight loss occurred at 361°C, which can be attributed to PLGA weight loss at 324°C, according to the literature (Singh et al., 2014). The thermal stability of PVA/PLGA-XN and PVA mats was similar. Possibly, xanthohumol, an organic compound, lowers the temperature at which the greatest weight loss occurred.

It is very important to highlight that PVA meshes with the incorporation of PLGA-XN NPs are quite stable at temperatures below 150°C, which is critical for future biomedical applications since human body temperature is the standard.

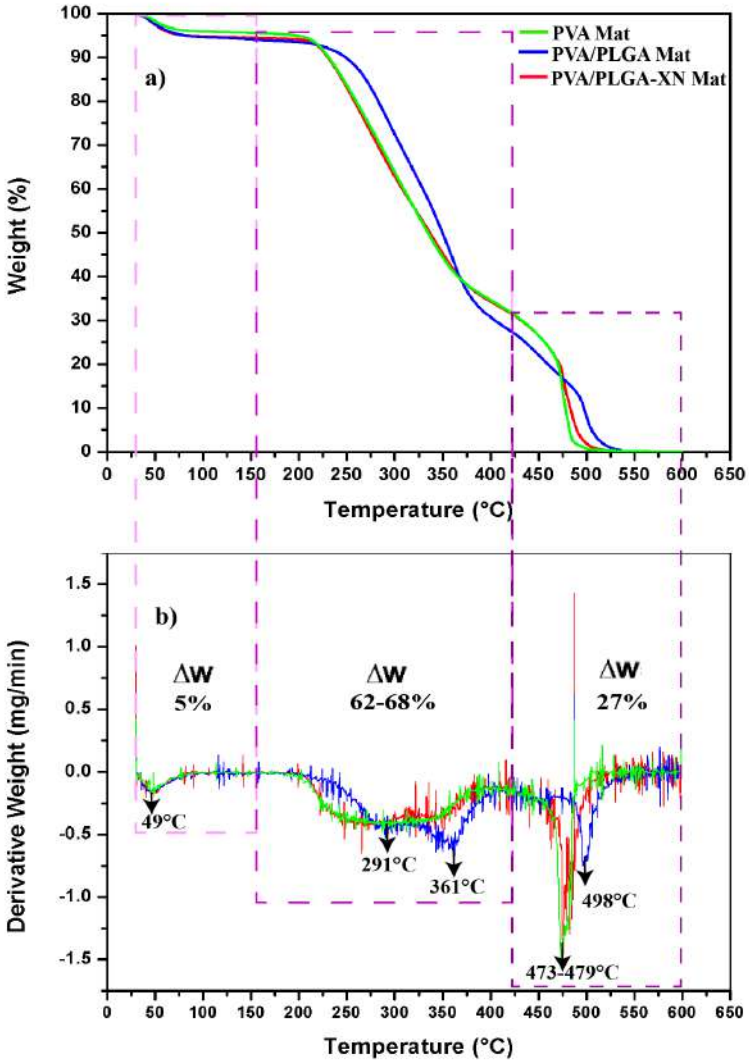


Figure 3.14: a) Thermogravimetric analysis (TGA) curves of PVA, PVA/PLGA, and PVA/PLGA-XN Mats and b) First derivative (DTG) graphs indicating the temperature at which the maximum weight loss happens.

## 3.3 Morphology of the Bimodal Scaffolds

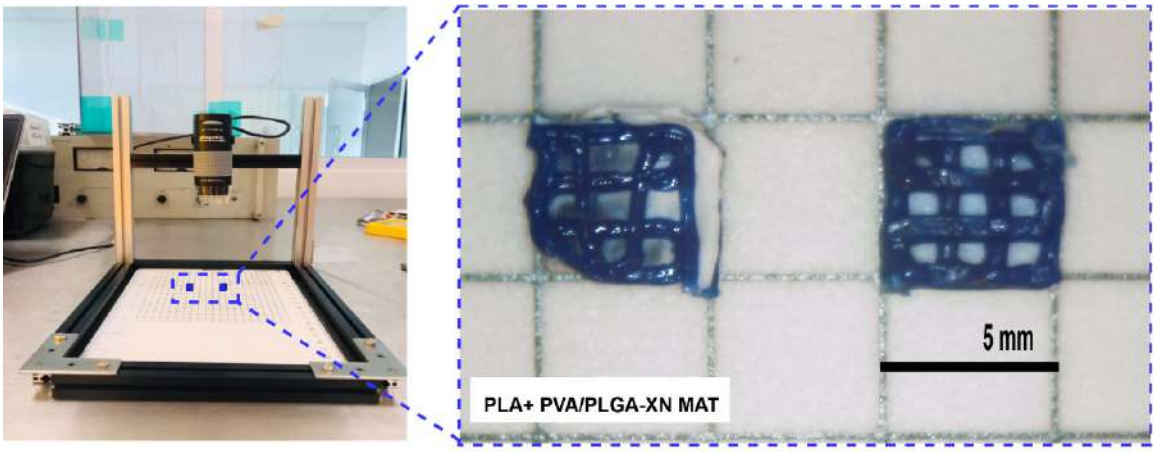


Figure 3.15: PLA Bimodal Scaffolds.

**Figure 3.15** shows the successful fabrication of bimodal scaffolds embedded with PVA/PLGA-XN NPs meshes. The morphology of the nonmodified PLA 3D constructs is presented in **Figure 3.16 a-c**. In these structures, morphological features were observed within design parameters derived from previous studies by Lara-Padilla et al. 2017. The pore size, strand diameter, and layer height were determined using ImageJ Software as shown in these micrographs. The results obtained were 898.78 $\mu$m $\pm$ 69.43, strand diameter 510.31 $\mu$m $\pm$ 34.96, and layer height 360.05 $\mu$m $\pm$ 34.93, respectively. **Figure 3.16 e-j** shows the morphology of bimodal scaffolds with PVA/PLGA-XN NPs meshes embedded. Mesh integrity was evident despite beads and drops of the polymer solution. It is possible that vertical electrospinning results in more droplets within the electrospun nanofibers. The cross-section morphology (**Figure 3.16 h-j**) confirmed the integration of the PVA/PLGA-XN inner layer. In general, the results confirmed the feasibility of manufacturing bimodal scaffolds. Furthermore, PVA meshes loaded with PLGA-XN NPs have a promising approach to biomedical applications.

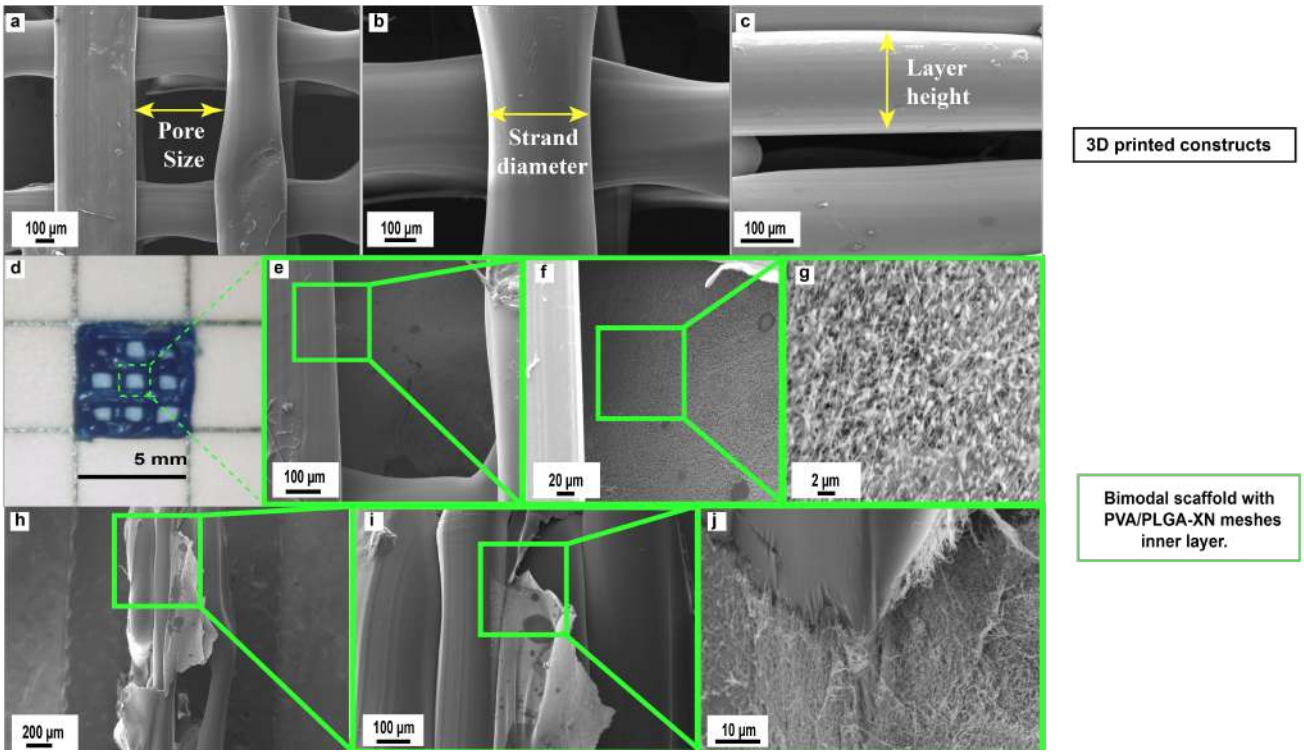


Figure 3.16: Morphology of 3D PLA constructs and bimodal scaffolds.

## 3.4 Cytotoxicity Assay

To support biological function and prevent rejection by body tissue, materials should be biocompatible. Physicochemical properties define biocompatibility, bioactivity, and safety. In this sense, size, chemical composition of the surface, shape, charge, and topography could influence the cell response (Gómez, Magaña, Bravo, Graziano, & Cai, 2022). **Based on Table 3.5**, XN reported cell viability of 67.93%, or approximately 30% mortality, suggesting a possible toxicity. Cell viability of the PVA meshes was 88.69% and for the PVA meshes with PLGA/XN NPs incorporated was 84.83%. These results confirmed the cytocompatibility of the meshes. In the study of Qiao et al. (2016) showed cell viability for fibrous membranes of PLGA and 10 wt%XN/PLGA of 86.66% and 78.42%, respectively.

In this study, the 3D PLA scaffolds showed a cell viability of 45.38%, and for bimodal scaffolds, it was 50.55%. A toxic effect was evident from the high mortality of the cells. Baran and Erbil (2019) explained that PLA is a relatively hydrophobic polymer that results in a low cell affinity in biomedical applications and sometimes it can cause an inflammatory response from the surrounding tissue with direct contact. According to Saniei and Mousavi (2020), PVA meshes had a higher cell viability than 3D PLA constructs. The electrospun PVA nanofiber coating improved the hydrophilicity of 3D-printed PLA screws. It also created a nano-pattern feature on the surface that mimicked the ECM, which is favorable for cellular attachment and proliferation. PVA meshes loaded with PLA/XN NPs increased the viability of bimodal scaffolds by approximately 5%. However, further investigation is required to confirm the results reported here.

Table 3.5: Viability percentage of fibroblasts with different treatments.

| **Treatments** | **Viability** (%) | **SD** (±) |
|---|---|---|
| Xanthohumol | 67.93 | 0.98 |
| PVA meshes | 88.69 | 1.97 |
| PVA/PLGA-XN NPs | 84.83 | 0.94 |
| 3D PLA scaffold | 45.38 | 1.32 |
| Bimodal scaffold | 50.55 | 4.92 |
| Control (Methanol) | 78.28 | 2.34 |

## 3.5 Potential Applications of the Proposed Bimodal Scaffolds

Periodontitis is an inflammatory disease caused by oral pathogens that affect the alveolar bone, periodontal ligament, cementum, and gingiva that support the teeth. Without a proper treatment, this disease can lead to the destruction of the periodontium and tooth loss, compromising the patient's health (J. dos Santos et al., 2021; D. M. dos Santos et al., 2022). Although the treatments currently used can limit the progression of the disease, alternative procedures are required when clinical therapies are not able to promote the complete regeneration of lost periodontal tissues (Hasani-Sadrabadi et al., 2019). It is necessary to design multifunctional and hierarchically structured biomaterials to achieve successful tissue regeneration because the periodontium consists of soft tissues (gingival ligaments and periodontal ligaments) and hard tissues (cementum and alveolar bone) (Vaquette et al., 2018). As a result, new scaffold manufacturing techniques are being developed to enhance tissue engineering functionality. In this regard, the potential application of the bimodal scaffolds presented here is for maxillofacial procedures, such as alveolar bone, where in *situ* drug delivery is desired to prevent the natural tendency for infections in the oral cavity.

PVA meshes can be used to create dense layers and provide barrier properties due to their densely packed arrangement (**Figure 3.17**). These meshes could mimic the ECM and facilitate a controlled release of the proposed compound (Xanthohumol) *in situ*. PVA is a synthetic polymer that has a very high potential for biomedical applications because of its biocompatibility, hydrophilicity, water retention properties, and fiber/film-forming properties (Bootdee & Nithitanakul, 2021). However, PVA nanofibers alone not are sufficient for therapeutic activity. For this reason, PVA mixture with natural extracts is one of the most effective methods for the preparation of compounds with specific properties (Bootdee & Nithitanakul, 2021; Torres-Martínez et al., 2020). The application of PLGA NPs as drug delivery systems has been widely investigated (Singh et al., 2014; Bootdee & Nithitanakul, 2021). Therefore, the incorporation of PLGA NPs into PVA nanofibers could be useful for the proposed application. Due to the polymeric matrix, encapsulated XN could have a controlled release and produce therapeutic effects in situ. For example, the incorporation of thermosensitive bioactive compounds is difficult through AM because the extrusion processes use high temperatures that can degrade these compounds (D. M. dos

Santos et al., 2022). Hence, the incorporation of meshes is essential to improving the performance of 3D-printed scaffolds in biomedical applications. The porous layer of PLA is intended to help in bone tissue regeneration and support electrospun meshes. The goal is that these bimodal scaffolds provide a microenvironment that promotes the regeneration of soft tissue and bone tissue, accelerating periodontal defect healing (Sowmya et al., 2017).

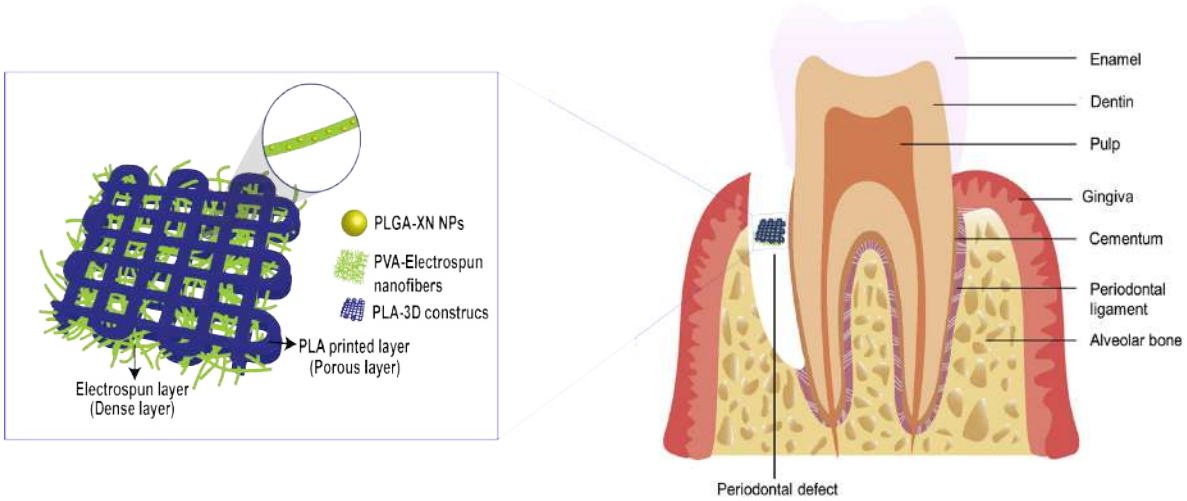


Figure 3.17: Potential aplication of the bimodal scaffolds (adapted from Liang et al. 2020).

About the nanostructured materials proposed here. Based on *in vitro* cytotoxicity tests, PVA/PLGA-XN meshes showed 84.83% viability, indicating cytocompatibility. The viability percentage of PLA constructs was 45.38%. According to the literature, materials composed entirely of this polymer (PLA) exhibit low biological activity and high hydrophilicity, limiting their ability to regenerate tissues (Hasani-Sadrabadi et al., 2019; Vaquette et al., 2018; D. M. dos Santos et al., 2022; Sowmya et al., 2017). The viability of PLA constructs increased to 50.55% when PVA/PLGA-XN meshes were incorporated. Despite the low viability of bimodal scaffolds, their potential applications cannot be discounted. *In vitro* cytotoxicity tests should be repeated to improve these results. For example, D. M. dos Santos et al. 2020 achieved viability percentages above 80& using commercial PLA filament and coating the construct with a curcumin-containing zein film before PCL electrospun meshes were deposited on the surface.

# Chapter 4

# Conclusions

This research showed that it is possible to manufacture PVA nanofibers with PLGA/XN NPs and that the methodology used is reproducible. The best parameters to fabricate nanostructured meshes were a concentration of 8.5% w/v, a flow rate of 0.2 mL/h, a collector distance between 13-14 cm, a voltage of 18 kV, and an electrospinning time of 20 minutes.

The synthesis of PLGA/XN NPs was validated by using a single emulsion method. According to DLS results, NPs filtration resulted in less agglomeration, small size, a better particle size distribution, and a negative surface charge, which is diserable to obtain a higher particle-particle repulsion and increase the formulation stability. The results obtained were a size distribution of 261.23 nm $\pm$ 2.51, polidispersity index of 0.26 $\pm$ 0.01 and a zeta potential of -16.07 mV $\pm$ 0.38.

In general, the morphology of PVA, PVA/PLGA, and PVA/PLGA-XN meshes by SEM showed the presence of beads and NPs. As a result of phase filtration, the scaffold morphology improved since beads formation decreased and a better distribution of NPs was observed. TEM analysis validated the incorporation of NPs into PVA electrospun nanofibers. Fluorescence microscopy results also demonstrated PLGA nanoparticles incorporated into nanofibers.

The FTIR analysis showed that the materials that make up the nanofibers do not chemically react with each other. For nanostructured materials with potential for drug delivery, this is desirable property. Electrospinning does not generate chemical changes in the components, thus only physical changes are observed. By FTIR, the absorption bands confirm that PVA is the polymer with the highest concentration. It is very important to highlight that PVA meshes with the incorporation of PLGA/XN NPs are quite stable at temperatures below 150°C, which is critical for future biomedical applications since human body temperature is the standard.

The morphology of the bimodal scaffolds demonstrated that the proposed meshes can be embedded into 3D PLA constructs through the combination of Fused Deposition Modeling and Electrospinning. Bimodal scaffolds were fabricated successfully in a square shape of 5x5 $mm^2$ with approximately 1 mm pore size and 0.4-0.5 mm layer height. The final design consisted of four layers of PLA strands and one layer of PVA/PLGA-XN

meshes. Our results validate the previous results obtained where bimodal scaffolds were produced.

*In vitro* cytotoxicity tests showed that PVA meshes with PLGA/XN NPs showed 84.83% viability, indicating cytocompatibility, which is encouraging for future research. The viability percentage of bimodal scaffolds was 50.55% compared to PLA constructs which were 45.38%. These showed that the incorporation of PVA/PLGA-XN meshes could improve the application of the 3D construct. Despite their low viability, bimodal scaffolds have potential applications. To improve these results, *in vitro* cytotoxicity tests should be repeated.

## 4.1 Contributions

This research has demonstrated and validated the feasibility to manufacture scaffolds with micro-nanostructured structures by the combination of manufacturing techniques. One of the most relevant contributions of this work was the encapsulation of a plant-derived compound (xanthohumol) obtained from the hop plant (*Humulus Lupulus L.*) into PLGA nanoparticles incorporated in PVA nanofibers meshes that can be used as drug delivery systems. This type of bimodal scaffold promises very interesting applications in tissue engineering and the biomedical sector. In addition, the use of different polymers may represent a means to achieve better control over the degradation kinetics and the release profile of the loaded bioactive agents.

## 4.2 Future Work

Considering the potential application of bimodal scaffolds in this study. It is necessary to conduct some studies in order to evaluate scaffold efficiency:

- *In vitro* cytotoxicity tests on bimodal scaffolds should be performed to improve the results reported in this study.
- Analysis of drug release of PLGA-XN nanoparticles by High-Performance Liquid Chromatography (HPLC).
- *In-vivo* testing of the scaffold.
- During periodontal regeneration therapy, infection prevention is crucial. Thus, it is important to examine the antibacterial efficacy of xanthohumol and the scaffolds obtained against a variety of periodontal pathogens.

# References


Adel, I. M., ElMeligy, M. F., & Elkasabgy, N. A. (2022, January). Conventional and Recent Trends of Scaffolds Fabrication: A Superior Mode for Tissue Engineering. *Pharmaceutics*, *14*(2), 306. Retrieved 2022-09-28, from https://www.mdpi.com/1999-4923/14/2/306 doi: 10.3390/pharmaceutics14020306

Akolpoğlu Başaran, D. D., Gündüz, U., Tezcaner, A., & Keskin, D. (2021). Topical delivery of heparin from plga nanoparticles entrapped in nanofibers of sericin/gelatin scaffolds for wound healing. *International Journal of Pharmaceutics*, *597*, 120207. Retrieved from https://www.sciencedirect.com/science/article/pii/S0378517321000119 doi: https://doi.org/10.1016/j.ijpharm.2021.120207

Ambrus, R., Alshweiat, A., Csóka, I., Ovari, G., Esmail, A., & Radacsi, N. (2019, August). 3D-printed electrospinning setup for the preparation of loratadine nanofibers with enhanced physicochemical properties. *International Journal of Pharmaceutics*, *567*, 118455. Retrieved 2022-10-01, from https://linkinghub.elsevier.com/retrieve/pii/S0378517319304892 doi: 10.1016/j.ijpharm.2019.118455

Auriemma, G., Tommasino, C., Falcone, G., Esposito, T., Sardo, C., & Aquino, R. P. (2022, April). Additive Manufacturing Strategies for Personalized Drug Delivery Systems and Medical Devices: Fused Filament Fabrication and Semi Solid Extrusion. *Molecules*, *27*(9), 2784. Retrieved 2022-10-01, from https://www.mdpi.com/1420-3049/27/9/2784 doi: 10.3390/molecules27092784

Banche-Niclot, F., Licini, C., Montalbano, G., Fiorilli, S., Mattioli-Belmonte, M., & Vitale-Brovarone, C. (2022, February). 3D Printed Scaffold Based on Type I Collagen/PLGA_tgf-1 Nanoparticles Mimicking the Growth Factor Footprint of Human Bone Tissue. *Polymers*, *14*(5), 857. Retrieved 2022-10-01, from https://www.mdpi.com/2073-4360/14/5/857 doi: 10.3390/polym14050857

Baran, E. H., & Erbil, H. Y. (2019). Surface modification of 3d printed pla objects by fused deposition modeling: A review. *Colloids and Interfaces*, *3*(2). Retrieved from https://www.mdpi.com/2504-5377/3/2/43 doi: 10.3390/colloids3020043

Batista, H., Freitas, J. P., Abrunheiro, A., Gonçalves, T., Gil, M. H., Figueiredo, M., & Coimbra, P. (2022, June). Electrospun composite fibers of PLA/PLGA blends and mesoporous silica nanoparticles for the controlled release of gentamicin sulfate. *International Journal of Polymeric Materials and Polymeric Biomaterials*, *71*(9), 635–646. Retrieved 2022-10-01, from https://www.tandfonline.com/doi/full/10.1080/00914037.2021.1876053 doi: 10.1080/00914037.2021.1876053

Belgheisi, G., Haghbin Nazarpak, M., & Solati-Hashjin, M. (2022, August). Fabrication and evaluation of combined 3D printed/pamidronate-layered double hydroxides enriched electrospun scaffolds for bone tissue engineering applications. *Applied Clay Science*, *225*, 106538. Retrieved 2022-10-01, from https://linkinghub.elsevier.com/retrieve/pii/S0169131722001338 doi: 10.1016/j.clay.2022.106538

Bootdee, K., & Nithitanakul, M. (2021, March). Poly( d,l -lactide-co-glycolide) nanospheres within composite poly(vinyl alcohol)/aloe vera electrospun nanofiber as a novel wound dressing for controlled release of drug. *International Journal of Polymeric Materials and Polymeric Biomaterials*, *70*(4), 223–230. Retrieved 2022-10-01, from https://www.tandfonline.com/doi/full/10.1080/00914037.2019.1706512 doi: 10.1080/00914037.2019.1706512

Böhm, C., Tandon, B., Hrynevich, A., Teßmar, J., & Dalton, P. D. (2022, March). Processing of Poly(lactic- *co* -glycolic acid) Microfibers via Melt Electrowriting. *Macromolecular Chemistry and Physics*, *223*(5), 2100417. Retrieved 2022-10-01, from https://onlinelibrary.wiley.com/doi/10.1002/macp.202100417 doi: 10.1002/macp.202100417

Centola, M., Rainer, A., Spadaccio, C., De Porcellinis, S., Genovese, J. A., & Trombetta, M. (2010, March). Combining electrospinning and fused deposition modeling for the fabrication of a hybrid vascular graft. *Biofabrication*, *2*(1), 014102. Retrieved 2022-10-01, from https://iopscience.iop.org/article/10.1088/1758-5082/2/1/014102 doi: 10.1088/1758-5082/2/1/014102

Chatterjee, M., & Chanda, N. (2022). Formulation of plga nano-carriers: specialized modification for cancer therapeutic applications. *Mater. Adv.*, *3*, 837-858. Retrieved from http://dx.doi.org/10.1039/D1MA00600B doi: 10.1039/D1MA00600B

Chou, Y.-C., Lee, D., Chang, T.-M., Hsu, Y.-H., Yu, Y.-H., Chan, E.-C., & Liu, S.-J. (2017, August). Combination of a biodegradable three-dimensional (3D) – printed cage for mechanical support and nanofibrous membranes for sustainable release of antimicrobial agents for treating the femoral metaphyseal comminuted fracture. *Journal of the Mechanical Behavior of Biomedical Materials*, *72*, 209–218. Retrieved 2022-10-01, from https://linkinghub.elsevier.com/retrieve/pii/S175161611730190X doi: 10.1016/j.jmbbm.2017.05.002

Chun, H. J., Park, C. H., Kwon, I. K., & Khang, G. (Eds.). (2018). *Cutting-Edge Enabling Technologies for Regenerative Medicine* (Vol. 1078). Singapore: Springer Singapore. Retrieved 2022-10-01, from http://link.springer.com/10.1007/978-981-13-0950-2 doi: 10.1007/978-981-13-0950-2

Ciapetti, G., Cenni, E., Pratelli, L., & Pizzoferrato, A. (1993). In vitro evaluation of cell/biomaterial interaction by mtt assay. *Biomaterials*, *14*(5), 359-364. Retrieved from https://www.sciencedirect.com/science/article/pii/0142961293900557 doi: https://doi.org/10.1016/0142-9612(93)90055-7

Dagtepe, P., & Chikan, V. (2010, 09). Quantized ostwald ripening of colloidal nanoparticles. *The Journal of Physical Chemistry C*, *114*. doi: 10.1021/jp105071a

Dalton, P. D., Vaquette, C., Farrugia, B. L., Dargaville, T. R., Brown, T. D., & Hutmacher, D. W. (2013). Electrospinning and additive manufacturing: converging technologies. *Biomater. Sci.*, *1*(2), 171–185. Retrieved 2022-10-01, from http://xlink.rsc.org/?DOI=C2BM00039C doi: 10.1039/C2BM00039C

Danhier, F., Ansorena, E., Silva, J. M., Coco, R., Le Breton, A., & Préat, V. (2012, July). PLGA-based nanoparticles: An overview of biomedical applications. *Journal of Controlled Release*, *161*(2), 505–522. Retrieved 2022-10-01, from https://linkinghub.elsevier.com/retrieve/pii/S0168365912000752 doi: 10.1016/j.jconrel.2012.01.043

dos Santos, D. M., de Annunzio, S. R., Carmello, J. C., Pavarina, A. C., Fontana, C. R., & Correa, D. S. (2022). Combining coaxial electrospinning and 3d printing: Design of biodegradable bilayered membranes with dual drug delivery capability for periodontitis treatment. *ACS Applied Bio Materials*, *5*(1), 146-159. Retrieved from https://doi.org/10.1021/acsabm.1c01019 (PMID: 35014831) doi: 10.1021/acsabm.1c01019

dos Santos, J., Oliveira, R. S., Oliveira, T. V., Velho, M. C., Konrad, M. V., da Silva, G. S., ... Beck, R. C. R. (2021, April). 3D Printing and Nanotechnology: A Multiscale Alliance in Personalized Medicine. *Advanced Functional Materials*, *31*(16), 2009691. Retrieved 2022-10-01, from https://onlinelibrary.wiley.com/doi/10.1002/adfm.202009691 doi: 10.1002/adfm.202009691

El-Fiqi, A., Kim, J.-H., & Kim, H.-W. (2015, January). Osteoinductive Fibrous Scaffolds of Biopolymer/Mesoporous Bioactive Glass Nanocarriers with Excellent Bioactivity and Long-Term Delivery of Osteogenic Drug. *ACS Applied Materials & Interfaces*, *7*(2), 1140–1152. Retrieved 2022-10-01, from https://pubs.acs.org/doi/10.1021/am5077759 doi: 10.1021/am5077759

Fonseca, M., Macedo, A. S., Lima, S. A. C., Reis, S., Soares, R., & Fonte, P. (2021, October). Evaluation of the Antitumour and Antiproliferative Effect of Xanthohumol-Loaded PLGA Nanoparticles on Melanoma. *Materials*, *14*(21), 6421. Retrieved 2022-10-01, from https://www.mdpi.com/1996-1944/14/21/6421 doi: 10.3390/ma14216421

Ghosh, A. K., Thapa, R., Hariani, H. N., Volyanyuk, M., Ogle, S. D., Orloff, K. A., ... Kaja, S. (2021, August). Poly(lactic-co-glycolic acid) Nanoparticles Encapsulating the Prenylated Flavonoid, Xanthohumol, Protect Corneal Epithelial Cells from Dry Eye Disease-Associated Oxidative Stress. *Pharmaceutics*, *13*(9), 1362. Retrieved 2022-10-01, from https://www.mdpi.com/1999-4923/13/9/1362 doi: 10.3390/pharmaceutics13091362

Gómez, L. J. V., Magaña, Y. T., Bravo, J. M. C., Graziano, R. V., & Cai, S. (2022, April). Cellular Responses to Nanomaterials with Biomedical Applications. *Journal of Nanomaterials*, *2022*, 1–3. Retrieved 2022-10-01, from https://www.hindawi.com/journals/jnm/2022/9823140/ doi: 10.1155/2022/9823140

Han, F., Wang, J., Ding, L., Hu, Y., Li, W., Yuan, Z., ... Li, B. (2020, March). Tissue Engineering and Regenerative Medicine: Achievements, Future, and Sustainability in Asia. *Frontiers in Bioengineering and Biotechnology*, *8*, 83. Retrieved 2022-10-01, from https://www.frontiersin.org/article/10.3389/fbioe.2020.00083/full doi: 10.3389/fbioe.2020.00083

Hasani-Sadrabadi, M. M., Sarrion, P., Nakatsuka, N., Young, T. D., Taghdiri, N., Ansari, S., ... Moshaverinia, A. (2019, April). Hierarchically Patterned Polydopamine-Containing Membranes for Periodontal Tissue Engineering. *ACS Nano*, *13*(4), 3830–3838. Retrieved 2022-10-01, from https://pubs.acs.org/doi/10.1021/acsnano.8b09623 doi: 10.1021/acsnano.8b09623

Hassan, M., Dave, K., Chandrawati, R., Dehghani, F., & Gomes, V. G. (2019, December). 3D printing of biopolymer nanocomposites for tissue engineering: Nanomaterials, processing and structure-function relation. *European Polymer Journal*, *121*, 109340. Retrieved 2022-10-01, from https://linkinghub.elsevier.com/retrieve/pii/S001430571931122X doi: 10.1016/j.eurpolymj.2019.109340

Hellerbrand. (2009, December). Xanthohumol, a prenylated chalcone derived from hops, inhibits proliferation, migration and interleukin-8 expression of hepatocellular carcinoma cells. *International Journal of Oncology*, *36*(2). Retrieved 2022-10-01, from http://www.spandidos-publications.com/ijo/36/2/435 doi: 10.3892/ijo_00000517

Hernández-Cruz, O., Avila-Gutierrez, L., Zolotukhin, M. G., Gonzalez, G., Monroy, B. M., Montiel, R., ... Massó Rojas, F. A. (2016, September). Spontaneous, Solvent-Free, Polymer-Templated, Solid–Solid Transformation of Thin Metal Films into Nanoparticles. *Nano Letters*, *16*(9), 5420–5425. Retrieved 2022-10-01, from https://pubs.acs.org/doi/10.1021/acs.nanolett.6b01780 doi: 10.1021/acs.nanolett.6b01780

Hou, S., Song, Y., Sun, D., Zhu, S., & Wang, Z. (2021, April). Xanthohumol-Induced Rat Glioma C6 Cells Death by Triggering Mitochondrial Stress. *International Journal of Molecular Sciences*, *22*(9), 4506. Retrieved 2022-10-01, from https://www.mdpi.com/1422-0067/22/9/4506 doi: 10.3390/ijms22094506

Hu, Y., Wang, J., Li, X., Hu, X., Zhou, W., Dong, X., ... Binks, B. P. (2019, June). Facile preparation of bioactive nanoparticle/poly(-caprolactone) hierarchical porous scaffolds via 3D printing of high internal phase Pickering emulsions. *Journal of Colloid and Interface Science*, *545*, 104–115. Retrieved 2022-10-01, from https://linkinghub.elsevier.com/retrieve/pii/S0021979719303157 doi: 10.1016/j.jcis.2019.03.024

Huang, B., Aslan, E., Jiang, Z., Daskalakis, E., Jiao, M., Aldalbahi, A., ... Bártolo, P. (2020, December). Engineered dual-scale poly (-caprolactone) scaffolds using 3D printing and rotational electrospinning for bone tissue regeneration. *Additive Manufacturing*, *36*, 101452. Retrieved 2022-10-01, from https://linkinghub.elsevier.com/retrieve/pii/S2214860420308241 doi: 10.1016/j.addma.2020.101452

Jammalamadaka, U., & Tappa, K. (2018, March). Recent Advances in Biomaterials for 3D Printing and Tissue Engineering. *Journal of Functional Biomaterials*, *9*(1), 22. Retrieved 2022-10-01, from https://www.mdpi.com/2079-4983/9/1/22 doi: 10.3390/jfb9010022

Jeong, H. M., Han, E. H., Jin, Y. H., Choi, Y. H., Lee, K. Y., & Jeong, H. G. (2011, May). Xanthohumol from the hop plant stimulates osteoblast differentiation by RUNX2 activation. *Biochemical and Biophysical Research Communications*, *409*(1), 82–89. Retrieved 2022-10-01, from https://linkinghub.elsevier.com/retrieve/pii/S0006291X1100711X doi: 10.1016/j.bbrc.2011.04.113

Kamsani, N. H., Haris, M. S., Pandey, M., Taher, M., & Rullah, K. (2021, July). Biomedical application of responsive 'smart' electrospun nanofibers in drug delivery system: A minireview. *Arabian Journal of Chemistry*, *14*(7), 103199. Retrieved 2022-10-01, from https://linkinghub.elsevier.com/retrieve/pii/S1878535221002148 doi: 10.1016/j.arabjc.2021.103199

Keloglu, N., Verrier, B., Trimaille, T., & Sohier, J. (2016, April). Controlled association and delivery of nanoparticles from jet-sprayed hybrid microfibrillar matrices. *Colloids and Surfaces B: Biointerfaces*, *140*, 142–149. Retrieved 2022-10-01, from https://linkinghub.elsevier.com/retrieve/pii/S092777651530388X doi: 10.1016/j.colsurfb.2015.12.039

Kim, B.-S., Yang, S.-S., & Kim, C. S. (2018, October). Incorporation of BMP-2 nanoparticles on the surface of a 3D-printed hydroxyapatite scaffold using an -polycaprolactone polymer emulsion coating method for bone tissue engineering. *Colloids and Surfaces B: Biointerfaces*, *170*, 421–429. Retrieved 2022-10-01, from https://linkinghub.elsevier.com/retrieve/pii/S0927776518304144 doi: 10.1016/j.colsurfb.2018.06.043

Kondiah, P. J., Kondiah, P. P. D., Choonara, Y. E., Marimuthu, T., & Pillay, V. (2020, February). A 3D Bioprinted Pseudo-Bone Drug Delivery Scaffold for Bone Tissue Engineering. *Pharmaceutics*, *12*(2), 166. Retrieved 2022-10-01, from https://www.mdpi.com/1999-4923/12/2/166 doi: 10.3390/pharmaceutics12020166

Kuchler-Bopp, S., Larrea, A., Petry, L., Idoux-Gillet, Y., Sebastian, V., Ferrandon, A., ... Benkirane-Jessel, N. (2017, March). Promoting bioengineered tooth innervation using nanostructured and hybrid scaffolds. *Acta Biomaterialia*, *50*, 493–501. Retrieved 2022-10-01, from https://linkinghub.elsevier.com/retrieve/pii/S1742706117300016 doi: 10.1016/j.actbio.2017.01.001

Kumar, R., Kumar, M., Tyagi, R., & Singh, R. (2022). Electrospinning Based Nanofibers for 3D Printing Applications. In *Encyclopedia of Materials: Plastics and Polymers* (pp. 253–263). Elsevier. Retrieved 2022-10-01, from https://linkinghub.elsevier.com/retrieve/pii/B9780128203521002479 doi: 10.1016/B978-0-12-820352-1.00247-9

Kunnimalaiyaan, S., Sokolowski, K. M., Balamurugan, M., Gamblin, T. C., & Kunnimalaiyaan, M. (2015, May). Xanthohumol Inhibits Notch Signaling and Induces Apoptosis in Hepatocellular Carcinoma. *PLOS ONE*, *10*(5), e0127464. Retrieved 2022-10-01, from https://dx.plos.org/10.1371/journal.pone.0127464 doi: 10.1371/journal.pone.0127464

Lara-Padilla, H., Mendoza-Buenrostro, C., Cardenas, D., Rodriguez-Garcia, A., & Rodriguez, C. (2017, June). Influence of Controlled Cooling in Bimodal Scaffold Fabrication Using Polymers with Different Melting Temperatures. *Materials*, *10*(6), 640. Retrieved 2022-10-01, from http://www.mdpi.com/1996-1944/10/6/640 doi: 10.3390/ma10060640

Lee, S.-J., Zhu, W., Heyburn, L., Nowicki, M., Harris, B., & Zhang, L. G. (2017, February). Development of Novel 3-D Printed Scaffolds With Core-Shell Nanoparticles for Nerve Regeneration. *IEEE Transactions on Biomedical Engineering*, *64*(2), 408–418.

Retrieved 2022-10-01, from http://ieeexplore.ieee.org/document/7460185/ doi: 10.1109/TBME.2016.2558493

Leonida, M. D., Belbekhouche, S., Benzecry, A., Peddineni, M., Suria, A., & Carbonnier, B. (2018, December). Antibacterial hop extracts encapsulated in nanochitosan matrices. *International Journal of Biological Macromolecules*, *120*, 1335–1343. Retrieved 2022-10-01, from https://linkinghub.elsevier.com/retrieve/pii/S0141813018324929 doi: 10.1016/j.ijbiomac.2018.09.003

Li, X., Wang, Y., Wang, Z., Qi, Y., Li, L., Zhang, P., ... Huang, Y. (2018, June). Composite PLA/PEG/nHA/Dexamethasone Scaffold Prepared by 3D Printing for Bone Regeneration. *Macromolecular Bioscience*, *18*(6), 1800068. Retrieved 2022-10-01, from https://onlinelibrary.wiley.com/doi/10.1002/mabi.201800068 doi: 10.1002/mabi.201800068

Liang, Y., Luan, X., & Liu, X. (2020). Recent advances in periodontal regeneration: A biomaterial perspective. *Bioactive Materials*, *5*(2), 297-308. Retrieved from https://www.sciencedirect.com/science/article/pii/S2452199X20300359 doi: https://doi.org/10.1016/j.bioactmat.2020.02.012

Lim, S. H., Kathuria, H., Tan, J. J. Y., & Kang, L. (2018, July). 3D printed drug delivery and testing systems — a passing fad or the future? *Advanced Drug Delivery Reviews*, *132*, 139–168. Retrieved 2022-10-01, from https://linkinghub.elsevier.com/retrieve/pii/S0169409X18301091 doi: 10.1016/j.addr.2018.05.006

Martin, V., Ribeiro, I. A., Alves, M. M., Gonçalves, L., Claudio, R. A., Grenho, L., ... Bettencourt, A. F. (2019, August). Engineering a multifunctional 3D-printed PLA-collagen-minocycline-nanoHydroxyapatite scaffold with combined antimicrobial and osteogenic effects for bone regeneration. *Materials Science and Engineering: C*, *101*, 15–26. Retrieved 2022-10-01, from https://linkinghub.elsevier.com/retrieve/pii/S0928493118335549 doi: 10.1016/j.msec.2019.03.056

Mayilswamy, N., Prakash, N. J., & Kandasubramanian, B. (2022). Design and fabrication of biodegradable electrospun nanofibers loaded with biocidal agents. *International Journal of Polymeric Materials and Polymeric Biomaterials*, *0*(0), 1-27. Retrieved from https://doi.org/10.1080/00914037.2021.2021905 doi: 10.1080/00914037.2021.2021905

Mendoza-Buenrostro, C., Lara, H., & Rodriguez, C. (2015). Hybrid Fabrication of a 3D Printed Geometry Embedded with PCL Nanofibers for Tissue Engineering Applications. *Procedia Engineering*, *110*, 128–134. Retrieved 2022-10-01, from https://linkinghub.elsevier.com/retrieve/pii/S1877705815012618 doi: 10.1016/j.proeng.2015.07.020

Mi, X., Wang, C., Sun, C., Chen, X., Huo, X., Zhang, Y., ... Li, J. (2017, May). Xanthohumol induces paraptosis of leukemia cells through p38 mitogen activated protein kinase signaling pathway. *Oncotarget*, *8*(19), 31297–31304. Retrieved 2022-10-01, from https://www.oncotarget.com/lookup/doi/10.18632/oncotarget.16185 doi: 10.18632/oncotarget.16185

Mohammadian, F., & Eatemadi, A. (2017, July). Drug loading and delivery using nanofibers scaffolds. *Artificial Cells, Nanomedicine, and Biotechnology*, *45*(5), 881–888. Retrieved 2022-10-01, from https://www.tandfonline.com/doi/full/10.1080/21691401.2016.1185726 doi: 10.1080/21691401.2016.1185726

Molina-Peña, R., Haji Mansor, M., Najberg, M., Thomassin, J.-M., Gueza, B., Alvarez-Lorenzo, C., ... Boury, F. (2021, December). Nanoparticle-containing electrospun nanofibrous scaffolds for sustained release of SDF-1. *International Journal of Pharmaceutics*, *610*, 121205. Retrieved 2022-10-01, from https://linkinghub.elsevier.com/retrieve/pii/S0378517321010115 doi: 10.1016/j.ijpharm.2021.121205

Moreno Madrid, A. P., Vrech, S. M., Sanchez, M. A., & Rodriguez, A. P. (2019, July). Advances in additive manufacturing for bone tissue engineering scaffolds. *Materials Science and Engineering: C*, *100*, 631–644. Retrieved 2022-10-01, from https://linkinghub.elsevier.com/retrieve/pii/S0928493118307938 doi: 10.1016/j.msec.2019.03.037

Mota, C., Puppi, D., Dinucci, D., Errico, C., Bártolo, P., & Chiellini, F. (2011, March). Dual-Scale Polymeric Constructs as Scaffolds for Tissue Engineering. *Materials*, *4*(3), 527–542. Retrieved 2022-10-01, from http://www.mdpi.com/1996-1944/4/3/527 doi: 10.3390/ma4030527

Naghieh, S., Foroozmehr, E., Badrossamay, M., & Kharaziha, M. (2017, November). Combinational processing of 3D printing and electrospinning of hierarchical poly(lactic acid)/gelatin-forsterite scaffolds as a biocomposite: Mechanical and biological assessment. *Materials & Design*, *133*, 128–135. Retrieved 2022-10-01, from https://linkinghub.elsevier.com/retrieve/pii/S0264127517307207 doi: 10.1016/j.matdes.2017.07.051

Ozbolat, I. T. (2015, May). Scaffold-Based or Scaffold-Free Bioprinting: Competing or Complementing Approaches? *Journal of Nanotechnology in Engineering and Medicine*, *6*(2), 024701. Retrieved 2022-10-01, from https://asmedigitalcollection.asme.org/nanoengineeringmedical/article doi: 10.1115/1.4030414

Park, Y., You, M., Shin, J., Ha, S., Kim, D., Heo, M. H., ... Seol, J. H. (2019, February). Thermal conductivity enhancement in electrospun poly(vinyl alcohol) and poly(vinyl alcohol)/cellulose nanocrystal composite nanofibers. *Scientific Reports*, *9*(1), 3026. Retrieved from https://doi.org/10.1038/s41598-019-39825-8 doi: 10.1038/s41598-019-39825-8

Patel, G. C., & Yadav, B. K. (2018). Polymeric nanofibers for controlled drug delivery applications. In *Organic Materials as Smart Nanocarriers for Drug Delivery* (pp. 147–175). Elsevier. Retrieved 2022-10-01, from https://linkinghub.elsevier.com/retrieve/pii/B978012813663800004X doi: 10.1016/B978-0-12-813663-8.00004-X

Piletska, E., Yawer, H., Canfarotta, F., Moczko, E., Smolinska-Kempisty, K., Piletsky, S., ... Piletsky, S. (2017, 12). Biomimetic silica nanoparticles prepared by a combination of solid-phase imprinting and ostwald ripening. *Scientific Reports*, *7*. doi: 10.1038/s41598-017-12007-0

Pina, S., Ribeiro, V. P., Marques, C. F., Maia, F. R., Silva, T. H., Reis, R. L., & Oliveira, J. M. (2019, June). Scaffolding Strategies for Tissue Engineering and Regenerative Medicine Applications. *Materials*, *12*(11), 1824. Retrieved 2022-10-01, from https://www.mdpi.com/1996-1944/12/11/1824 doi: 10.3390/ma12111824

Plazar, J., Žegura, B., Lah, T. T., & Filipič, M. (2007, August). Protective effects of xanthohumol against the genotoxicity of benzo(a)pyrene (BaP), 2-amino-3-methylimidazo[4,5-f]quinoline (IQ) and tert-butyl hydroperoxide (t-BOOH)

in HepG2 human hepatoma cells. *Mutation Research/Genetic Toxicology and Environmental Mutagenesis*, *632*(1-2), 1–8. Retrieved 2022-10-01, from https://linkinghub.elsevier.com/retrieve/pii/S1383571807001568 doi: 10.1016/j.mrgentox.2007.03.013

Pouroutzidou, G. K., Lazaridou, M., Papoulia, C., Tsamesidis, I., Chrissafis, K., Vourlias, G., ... Kontonasaki, E. (2022, March). Electrospun PLGA Membranes with Incorporated Moxifloxacin-Loaded Silica-Based Mesoporous Nanocarriers for Periodontal Regeneration. *Nanomaterials*, *12*(5), 850. Retrieved 2022-10-01, from https://www.mdpi.com/2079-4991/12/5/850 doi: 10.3390/nano12050850

Puppi, D., & Chiellini, F. (2020, September). Biodegradable Polymers for Biomedical Additive Manufacturing. *Applied Materials Today*, *20*, 100700. Retrieved 2022-10-01, from https://linkinghub.elsevier.com/retrieve/pii/S2352940720301475 doi: 10.1016/j.apmt.2020.100700

Qiao, T., Jiang, S., Song, P., Song, X., Liu, Q., Wang, L., & Chen, X. (2016, October). Effect of blending HA-g-PLLA on xanthohumol-loaded PLGA fiber membrane. *Colloids and Surfaces B: Biointerfaces*, *146*, 221–227. Retrieved 2022-10-01, from https://linkinghub.elsevier.com/retrieve/pii/S0927776516304416 doi: 10.1016/j.colsurfb.2016.06.011

Rajzer, I., Kurowska, A., Jabłoński, A., Jatteau, S., Śliwka, M., Ziabka, M., & Menaszek, E. (2018, October). Layered gelatin/PLLA scaffolds fabricated by electrospinning and 3D printing- for nasal cartilages and subchondral bone reconstruction. *Materials & Design*, *155*, 297–306. Retrieved 2022-10-01, from https://linkinghub.elsevier.com/retrieve/pii/S0264127518304799 doi: 10.1016/j.matdes.2018.06.012

Rogers, C. M., Morris, G. E., Gould, T. W. A., Bail, R., Toumpaniari, S., Harrington, H., ... Rose, F. R. A. J. (2014, April). A novel technique for the production of electrospun scaffolds with tailored three-dimensional micro-patterns employing additive manufacturing. *Biofabrication*, *6*(3), 035003. Retrieved 2022-10-01, from https://iopscience.iop.org/article/10.1088/1758-5082/6/3/035003 doi: 10.1088/1758-5082/6/3/035003

Rosenberg, M., Shilo, D., Galperin, L., Capucha, T., Tarabieh, K., Rachmiel, A., & Segal, E. (2019, November). Bone Morphogenic Protein 2-Loaded Porous Silicon Carriers for Osteoinductive Implants. *Pharmaceutics*, *11*(11), 602. Retrieved 2022-10-01, from https://www.mdpi.com/1999-4923/11/11/602 doi: 10.3390/pharmaceutics11110602

Rouhollahi, F., Hosseini, S. A., Alihosseini, F., Allafchian, A., & Haghighat, F. (2018, October). Investigation on the Biodegradability and Antibacterial Properties of Nanohybrid Suture Based on Silver Incorporated PGA-PLGA Nanofibers. *Fibers and Polymers*, *19*(10), 2056–2065. Retrieved 2022-10-01, from http://link.springer.com/10.1007/s12221-018-8316-7 doi: 10.1007/s12221-018-8316-7

Ruiz-Esparza, G. U., Wu, S., Segura-Ibarra, V., Cara, F. E., Evans, K. W., Milosevic, M., ... Blanco, E. (2014, August). Polymer Nanoparticles Encased in a Cyclodextrin Complex Shell for Potential Site- and Sequence-Specific Drug Release. *Advanced Functional Materials*, *24*(30), 4753–4761. Retrieved 2022-10-01, from https://onlinelibrary.wiley.com/doi/10.1002/adfm.201400011 doi: 10.1002/adfm.201400011

Sanchez-Alvarado, D., Guzmán-Pantoja, J., Páramo-García, U., Maciel-Cerda, A., Martínez-Orozco, R., & Vera-Graziano, R. (2018, June). Morphological Study of Chitosan/Poly (Vinyl Alcohol) Nanofibers Prepared by Electrospinning, Collected on Reticulated Vitreous Carbon. *International Journal of Molecular Sciences*, *19*(6), 1718. Retrieved 2022-10-01, from http://www.mdpi.com/1422-0067/19/6/1718 doi: 10.3390/ijms19061718

Saniei, H., & Mousavi, S. (2020, May). Surface modification of PLA 3D-printed implants by electrospinning with enhanced bioactivity and cell affinity. *Polymer*, *196*, 122467. Retrieved 2022-10-01, from https://linkinghub.elsevier.com/retrieve/pii/S0032386120303025 doi: 10.1016/j.polymer.2020.122467

Senthamizhan, A., Balusamy, B., & Uyar, T. (2017). Electrospinning. In *Electrospun Materials for Tissue Engineering and Biomedical Applications* (pp. 3–41). Elsevier. Retrieved 2022-10-01, from https://linkinghub.elsevier.com/retrieve/pii/B9780081010228000016 doi: 10.1016/B978-0-08-101022-8.00001-6

Sequeira, J. A., Pereira, I., Ribeiro, A. J., Veiga, F., & Santos, A. C. (2020). Surface functionalization of PLGA nanoparticles for drug delivery. In *Handbook of Functionalized Nanomaterials for Industrial Applications* (pp. 185–203). Elsevier. Retrieved 2022-10-01, from https://linkinghub.elsevier.com/retrieve/pii/B9780128167878000089 doi: 10.1016/B978-0-12-816787-8.00008-9

Shaw, G., & Samavedi, S. (2021, 12). Potent particle-based vehicles for growth factor delivery from electrospun meshes: Fabrication and functionalization strategies for effective tissue regeneration. *ACS Biomaterials Science Engineering*, *8*. doi: 10.1021/acsbiomaterials.1c00942

Singh, G., Tanurajvir, K., Ravinder, K., & Kaur, A. (2014, 01). Recent biomedical applications and patents on biodegradable polymer-plga. *International Journal of Pharmacology and Pharmaceutical Sciences*, *1*, 30-42.

Smith, J. A., & Mele, E. (2021, November). Electrospinning and Additive Manufacturing: Adding Three-Dimensionality to Electrospun Scaffolds for Tissue Engineering. *Frontiers in Bioengineering and Biotechnology*, *9*, 674738. Retrieved 2022-10-01, from https://www.frontiersin.org/articles/10.3389/fbioe.2021.674738/full doi: 10.3389/fbioe.2021.674738

Sowmya, S., Mony, U., Jayachandran, P., Reshma, S., Kumar, R. A., Arzate, H., ... Jayakumar, R. (2017, April). Tri-Layered Nanocomposite Hydrogel Scaffold for the Concurrent Regeneration of Cementum, Periodontal Ligament, and Alveolar Bone. *Advanced Healthcare Materials*, *6*(7), 1601251. Retrieved 2022-10-01, from https://onlinelibrary.wiley.com/doi/10.1002/adhm.201601251 doi: 10.1002/adhm.201601251

Stewart, S., Domínguez-Robles, J., McIlorum, V., Mancuso, E., Lamprou, D., Donnelly, R., & Larrañeta, E. (2020, January). Development of a Biodegradable Subcutaneous Implant for Prolonged Drug Delivery Using 3D Printing. *Pharmaceutics*, *12*(2), 105. Retrieved 2022-10-01, from https://www.mdpi.com/1999-4923/12/2/105 doi: 10.3390/pharmaceutics12020105

Sun, X., Xu, C., Wu, G., Ye, Q., & Wang, C. (2017, June). Poly(Lactic-co-Glycolic Acid): Applications and Future Prospects for Periodontal Tissue Regeneration. *Polymers*, *9*(12), 189. Retrieved 2022-10-01, from http://www.mdpi.com/2073-4360/9/6/189 doi: 10.3390/polym9060189

Surassmo, S., Saengkrit, N., Ruktanonchai, U. R., Suktham, K., Woramongkolchai, N., Wutikhun, T., & Puttipipatkhachorn, S. (2015). Surface modification of plga nanoparticles by carbopol to enhance mucoadhesion and cell internalization. *Colloids and Surfaces B: Biointerfaces*, *130*, 229-236. Retrieved from https://www.sciencedirect.com/science/article/pii/S0927776515002295 doi: https://doi.org/10.1016/j.colsurfb.2015.04.015

Teixeira, M. A., Amorim, M. T. P., & Felgueiras, H. P. (2020). Poly(vinyl alcohol)-based nanofibrous electrospun scaffolds for tissue engineering applications. *Polymers*, *12*(1). Retrieved from https://www.mdpi.com/2073-4360/12/1/7 doi: 10.3390/polym12010007

Torres-Martinez, E. J., Pérez-González, G. L., Serrano-Medina, A., Grande, D., Vera-Graziano, R., Cornejo-Bravo, J. M., & Villarreal-Gómez, L. J. (2019, July). Drugs Loaded into Electrospun Polymeric Nanofibers for Delivery. *Journal of Pharmacy & Pharmaceutical Sciences*, *22*, 313–331. Retrieved 2022-10-01, from https://journals.library.ualberta.ca/jpps/index.php/JPPS/article/view/29674 doi: 10.18433/jpps29674

Torres-Martínez, E. J., Vera-Graziano, R., Cervantes-Uc, J. M., Bogdanchikova, N., Olivas-Sarabia, A., Valdez-Castro, R., ... Villarreal-Gómez, L. J. (2020, December). Preparation and characterization of electrospun fibrous scaffolds of either PVA or PVP for fast release of sildenafil citrate. *e-Polymers*, *20*(1), 746–758. Retrieved 2022-10-01, from https://www.degruyter.com/document/doi/10.1515/epoly-2020-0070/html doi: 10.1515/epoly-2020-0070

Turnbull, G., Clarke, J., Picard, F., Riches, P., Jia, L., Han, F., ... Shu, W. (2018, September). 3D bioactive composite scaffolds for bone tissue engineering. *Bioactive Materials*, *3*(3), 278–314. Retrieved 2022-10-01, from https://linkinghub.elsevier.com/retrieve/pii/S2452199X17300397 doi: 10.1016/j.bioactmat.2017.10.001

Vaquette, C., Pilipchuk, S. P., Bartold, P. M., Hutmacher, D. W., Giannobile, W. V., & Ivanovski, S. (2018, November). Tissue Engineered Constructs for Periodontal Regeneration: Current Status and Future Perspectives. *Advanced Healthcare Materials*, *7*(21), 1800457. Retrieved 2022-10-01, from https://onlinelibrary.wiley.com/doi/10.1002/adhm.201800457 doi: 10.1002/adhm.201800457

Vazquez-Armendariz, J., Tejeda-Alejandre, R., Rodriguez-Garcia, A., Vega-Cantu, Y. I., Mendoza-Buenrostro, C., & Rodriguez, C. A. (2020, June). Influence of Controlled Cooling on Crystallinity of Poly(L-Lactic Acid) Scaffolds after Hydrolytic Degradation. *Materials*, *13*(13), 2943. Retrieved 2022-10-01, from https://www.mdpi.com/1996-1944/13/13/2943 doi: 10.3390/ma13132943

Villarreal-Gómez, L. J., Cornejo-Bravo, J. M., Vera-Graziano, R., & Grande, D. (2016, January). Electrospinning as a powerful technique for biomedical applications: a critically selected survey. *Journal of Biomaterials Science, Polymer Edition*, *27*(2),

157–176. Retrieved 2022-10-01, from http://www.tandfonline.com/doi/full/10.1080/09205063.2015.1116885 doi: 10.1080/09205063.2015.1116885

Vyas, C., Ates, G., Aslan, E., Hart, J., Huang, B., & Bartolo, P. (2020, June). Three-Dimensional Printing and Electrospinning Dual-Scale Polycaprolactone Scaffolds with Low-Density and Oriented Fibers to Promote Cell Alignment. *3D Printing and Additive Manufacturing*, *7*(3), 105–113. Retrieved 2022-10-01, from https://www.liebertpub.com/doi/10.1089/3dp.2019.0091 doi: 10.1089/3dp.2019.0091

Vázquez, N., Sánchez-Arévalo, F., Maciel-Cerda, A., Garnica-Palafox, I., Ontiveros-Tlachi, R., Chaires-Rosas, C., ... Castell-Rodríguez, A. (2019, May). Influence of the PLGA/gelatin ratio on the physical, chemical and biological properties of electrospun scaffolds for wound dressings. *Biomedical Materials*, *14*(4), 045006. Retrieved 2022-10-01, from https://iopscience.iop.org/article/10.1088/1748-605X/ab1741 doi: 10.1088/1748-605X/ab1741

Wang, Z., Wang, Y., Yan, J., Zhang, K., Lin, F., Xiang, L., ... Zhang, H. (2021, July). Pharmaceutical electrospinning and 3D printing scaffold design for bone regeneration. *Advanced Drug Delivery Reviews*, *174*, 504–534. Retrieved 2022-10-01, from https://linkinghub.elsevier.com/retrieve/pii/S0169409X21001630 doi: 10.1016/j.addr.2021.05.007

Xu, X. F. (2012, November). Preparation and *In Vitro* Degradation of PLGA/HA Composite Fiber Scaffolds by Electrospinning. *Advanced Materials Research*, *591-593*, 982–988. Retrieved 2022-10-01, from https://www.scientific.net/AMR.591-593.982 doi: 10.4028/www.scientific.net/AMR.591-593.982

Yang, T., Hu, Y., Wang, C., & Binks, B. P. (2017, July). Fabrication of Hierarchical Macroporous Biocompatible Scaffolds by Combining Pickering High Internal Phase Emulsion Templates with Three-Dimensional Printing. *ACS Applied Materials & Interfaces*, *9*(27), 22950–22958. Retrieved 2022-10-01, from https://pubs.acs.org/doi/10.1021/acsami.7b05012 doi: 10.1021/acsami.7b05012

Yu, Y., Hua, S., Yang, M., Fu, Z., Teng, S., Niu, K., ... Yi, C. (2016). Fabrication and characterization of electrospinning/3D printing bone tissue engineering scaffold. *RSC Advances*, *6*(112), 110557–110565. Retrieved 2022-10-01, from http://xlink.rsc.org/?DOI=C6RA17718B doi: 10.1039/C6RA17718B

Zhang, L., Yang, G., Johnson, B. N., & Jia, X. (2019, January). Three-dimensional (3D) printed scaffold and material selection for bone repair. *Acta Biomaterialia*, *84*, 16–33. Retrieved 2022-10-01, from https://linkinghub.elsevier.com/retrieve/pii/S1742706118307025 doi: 10.1016/j.actbio.2018.11.039

Zhang, X., Han, L., Sun, Q., Xia, W., Zhou, Q., Zhang, Z., & Song, X. (2020, March). Controlled release of resveratrol and xanthohumol via coaxial electrospinning fibers. *Journal of Biomaterials Science, Polymer Edition*, *31*(4), 456–471. Retrieved 2022-10-01, from https://www.tandfonline.com/doi/full/10.1080/09205063.2019.1700600 doi: 10.1080/09205063.2019.1700600

Zhao, W., Li, J., Jin, K., Liu, W., Qiu, X., & Li, C. (2016, February). Fabrication of functional PLGA-based electrospun scaffolds and their applications in biomedical

engineering. *Materials Science and Engineering: C*, *59*, 1181–1194. Retrieved 2022-10-01, from https://linkinghub.elsevier.com/retrieve/pii/S0928493115305579 doi: 10.1016/j.msec.2015.11.026